Coefficients for the calculation of thermophysical properties of indolene/ethanol biofuels for transcritical engine simulations

Coefficients for the Calculation of Thermophysical Properties of Indolene/Ethanol Biofuels for Transcritical Engine Simulations

Sergio Negro [a, b], Stefania Falfari [a], and Gian Marco Bianchi [a]

([a]) Department of Industrial Engineering, School of Engineering and Architecture, University of Bologna, Viale Risorgimento 2, 40136 – Bologna, Italy

([b]) Visiting Scientist at Engine Research and Development Laboratory (ERDL), Faculty of Applied Science and Engineering, University of Toronto, Toronto, ON, Canada

Corresponding author's contact information:

Dr. Sergio Negro

Mail Address: Mechanical and Industrial Engineering, Faculty of Applied Science and Engineering, University of Toronto, 5 King's College Road, Toronto, ON, Canada M5S 3G8 (MC 105)

e-mail: sergio.negro@utoronto.ca

Co-author's e-mail addresses: Prof. Gian Marco Bianchi, gianmarco.bianchi@unibo.it; Dr. Stefania Falfari, stefania.falfari@unibo.it.

Abstract

Driven by fuel economy and emission control concerns, modern automotive internal combustion engines operate at increasingly higher pressures and temperatures. The development of new low emission advanced combustion concepts relies on accurate predictions of the fuel mixture formation and combustion, sometimes near or across the critical point of the fuel blend. The present work provides libraries of thermodynamic and transport properties of automotive certification fuel surrogate, indolene, and its mixtures with ethanol E5, E10, E15, E20, E25, E50 and E85, to be used in the subcritical and supercritical range, in order to make transcritical fuel predictions possible and accurate.

Values of enthalpy, latent heat of vaporization, isobaric and isochoric specific heat capacity, entropy, surface tension, thermal conductivity, density, vapour pressure and viscosity are obtained numerically through theoretical and semi-empirical correlations and given for all the specified mixtures in the form of polynomial functions of temperature. The synthesis of the coefficients was obtained by minimizing the least-squares-errors through a 5^{th} order polynomial regression fit method. This format is particularly convenient for implementing computer equations or for use in CFD numerical codes.

Keywords: thermodynamic and transport properties; transcritical fluid dynamic simulation; supecritical injection; non-ideal blends; biofuel; internal combustion engines.

1. Introduction

Gasoline-Ethanol blends are used in large scale, worldwide, as biofuels. Most governments have introduced alternative fuel road maps with various legislation which are intended to promote and increase the use of biofuels in the next decades. At present, up to 10 % ethanol in standard gasoline can be found in U.S., Canada, most European countries, and high-level ethanol-gasoline blend containing 51%-83% ethanol by volume, named E85 or flex fuel, is largely available in Brazil, and sold in smaller amount in the U.S.; the latter two countries are the major producers and exporters of ethanol as biofuel. In U.S., blender pumps are also commonly available; these special pumps draw fuel from two separate storage tanks (E10 and E85) and can dispense E15, E20 and any other blend of those two fuels to flexible fuel vehicles (FFV). Notwithstanding the deep and global diffusion of ethanol-gasoline blends, there is a relatively small amount of data available in terms of thermophysical properties of these fuels in technical literature in the subcritical range, and no data present at all in the near-critical or supercritical range.

Currently, supercritical fluids are involved in numerous scientific and industrial applications, especially related to energy production or transfer. The necessity of developing high efficiency combustion engines made supercritical conditions the matter of study in spray formation, mixture formation, and combustion technology. Examples of studies consider liquid-propellant rockets, advanced aircraft gas turbines, and modern Diesel engines. Transcritical combustion involving subcritical to supercritical transition of fluids is intensively studied in cryogenic rocket engine research, where cryogenic oxygen, hydrogen or methane, are injected in a transcritical or supercritical state [1]. Supercritical fuels have been studied in relation to gasoline engines as well [2], through a process called 'Transonic Combustion' in which, the authors stated, a fuel injected in supercritical state into the combustion chamber allows for a rapid mixing with the chamber contents, and promotes high rates of heat release increasing the overall engine efficiency. The process is actually an injection-ignition process, similar to that of a Diesel engine, which, furthermore, allows the engine to operate un-throttled.

In transcritical combustion the reactants, which may be injected in a subcritical state, are subject to a rapid increase in temperature. This variation can be extremely large, in the order of thousands kelvin. When the fluid's behaviour is numerically simulated its characteristics need to be predicted over the whole range of temperatures and through the critical point.

The importance of accurately describing thermodynamic properties, non-ideality, and supercritical conditions in fuel injection processes is confirmed by the recent work of L. Qiu and R. D. Reitz [3]. In

their study they simulated supercritical-to-supercritical and supercritical-to-subcritical fuel injections, investigating the heat transfer interactions and the possibility of fuel condensation.
Other advanced combustion concepts for internal combustion engines, such as homogeneous charge compression ignition (HCCI), premixed charge compression ignition (PCCI), and spark-ignition direct injection engines (SIDI) with flash boiling sprays [4], involve fuel injection processes where temperatures and pressures are increasingly higher compared to past injection and ignition systems and their investigation, due to the complexity of a real fuel composition and the presence of low boiling point aromatics and alcohols, may also benefit from a detailed near-critical point description of the thermodynamic and transport properties of the biofuel injected. In substance, near-critical and transcritical behaviour may play a considerable role in current fluid dynamics and combustion simulations which involve a large variation in the thermal conditions of the fuel itself.
According to classical thermodynamic theory, a fluid is in a supercritical state when it is at a pressure and temperature above its critical point. These fluids show characteristics resembling both liquids and gases. The knowledge of their thermo-physical properties is still partially unclear because direct observation of supercritical fluids is a hard and expensive task. Numerical simulations, on the other hand, are a convenient approach to the problem of transcritical behaviour, as they can provide a substantial amount of information at relatively low cost and time.
The choice of a certification fuel, indolene, as a base fuel instead of a commercial gasoline was made to increase the reliability and reproducibility of the tests as indolene has a well defined composition with a very limited number of components that can accurately be reproduced, in contrast to gasoline that is instead constituted by hundreds of components and may present a large batch to batch variability. Furthermore, certification fuels are well documented in technical literature, while the actual compositions of commercial gasoline are usually unknown. As a result, calculations performed with certification fuels represent the only viable option linking engine simulations to experimental testing.
Libraries of thermodynamic data and transport properties were given in the past for a large number of individual species by McBride and Gordon (1993) [5] and R.A. Svehla (1995) [6] but not for mixtures; furthermore, those properties were obtained for gases only and there is no attempt in literature of providing libraries of thermophysical properties of certification and oxygenated fuels for the automotive industry capable of describing a transcritical biofuel behaviour. The present work attempts to fill this gap in the rapidly evolving automotive industry.
In this work, most of the properties were calculated by using thermodynamic fundamental relations combined with the Peng-Robinson equation of state [7]; the distillation curves were obtained by

solving numerically the Rachford-Rice equation [8]. The Wilson model for the calculation of the activity coefficients was applied to both the calculation of the vapour pressure and the distillation curves [9]. The concept of departure functions was applied to calculate real enthalpy, isobaric and isocoric specific heat capacity, latent heat of vaporization, and entropy. A combined Sastri et Rao [10] and Pitzer [11] model was used for the surface tension, a typical polynomial function with the coefficients proposed by McBride et al. [5] and from the Cheric database [12] were used for the thermal conductivity of gases, while a modified Latini et al. model [13] was employed for calculating the thermal conductivity of liquids. Based on the similarity of PvT and TμP relationships, a PT-μ viscosity equation was implemented and solved for viscosity of liquid, vapour, and supercritical phase, following the recommendation and the viscosity corrections proposed by Tian-Bo Fan and Li-Sheng Wang [14].

The calculated properties of numerically modelled indolene, E5, E10, E15, E20, E25, and E85 were synthesized into polynomial functions of the temperature, through a 5^{th} order polynomial regression fit method which minimizes the least-squares errors of the fit.

The work is organized as follow: first the models for calculating each property are explained and their validation versus technical data available from literature is shown. Second, the synthesis of the surrogate model for indolene and its blends with ethanol is proposed and validation based on the distillation curves and Reid Vapour Pressure (RVP) is presented. Third, the results from calculations were used to extract the coefficients for the polynomial functions of the thermophysical properties in object, by using a least squares regression fit method.

2. Thermophysical modelling

2.1 The Peng Robinson equation of state (PR-EOS)

Surrogates can be designed and optimized to describe particular fuel characteristics or engine processes, such as evaporation rate and spray formation, heat transfer, combustion and emissions. In the present work a multi-component model is employed in which a limited number of components is adopted to match the actual fuel properties. It is well known that adding ethanol or methanol to gasoline produces an increase in the vapour pressure of the blend and generates azeotropic mixtures, where the blend shows only one boiling point. In the present work a procedure able to deal with this non-ideal behaviour of hydrocarbon/alcohol blends is used and described in this section. The fundamental properties of the biofuel surrogates are modelled by using the Peng-Robinson equation of state. The Peng–Robinson equation of state was developed in 1976 specifically for petroleum

calculations and offers very good predictions when dealing with hydrocarbons, also across the critical point. It can be used in conjunction with mixing rules to describe complex mixtures and performs better than other cubic EOS (RK, SRK) also in the supercritical region. This equation reads for a pure component [7]

$$P = \frac{RT}{v-b} - \frac{a(T,\omega)}{v(v+b)+b(v-b)} \qquad (1)$$

where the attractive term is function of the temperature T and the acentric factor ω

$$a(T,\omega) = 0.45724 \frac{R^2 T_C^2}{P_C} \left[1 + k(\omega)\left(1 - \sqrt{T_r}\right)\right]^2 \qquad (2)$$

$$k(\omega) = 0.37464 + 1.54226\omega - 0.26992\omega^2 \qquad (3)$$

At the critical point, $a_c = 0.45724 \frac{R^2 T_C^2}{P_C}$ and the co-volume is expressed by $b = 0.07780 \frac{RT_C}{P_C}$.

By expressing the equation of state in a generalized form, the compressibility factor can be expressed as $Z = \frac{Pv}{RT}$, and setting $B = \frac{bP}{RT}$, $A = \frac{aP}{R^2T^2}$, the PvT equation becomes cubic in Z

$$Z^3 - Z^2(1-B) + Z\left(A - 3B^2 - B\right) - \left(AB - B^2 - B^3\right) = 0 \qquad (4)$$

The largest real solution represents the compressibility of the vapour phase and the smallest solution belongs to the liquid phase. The intermediate solution does not have a physical meaning and it is discarded. Above the critical point, only one real solution is obtained by equation (4).

For applying this equation of state to surrogate mixtures, mixing rules are needed to calculate the terms *a(T)* and *b* for the blends. In the present work the classic van der Waals mixing rules are adopted. This set of rules are well suited for components which properties are not too dissimilar. In the present work they are used for the calculation of average properties of the hydrocarbon surrogate, namely indolene. For a mixture of N-components they are expressed as

$$a_m = \sum_{i=1}^{N} \sum_{j=1}^{N} x_i x_j \left(a_i a_j\right)^{\frac{1}{2}} \left(1 - k_{ij}\right) \qquad (5)$$

$$b_m = \sum_{i=1}^{N}\sum_{j=1}^{N} x_i x_j \left(\frac{b_i + b_j}{2}\right)\left(1 - d_{ij}\right) \qquad (6)$$

where x_k represents the mole fraction of the k-component in a mixture, k_{ij} and d_{ij} are binary interaction parameters which considers molecular interactions between pairs of components. Both parameters k_{ij} and d_{ij} can be set equal to zero with good approximation when mixing non-polar substances such as hydrocarbons. The values of a_m and b_m can be used to calculate the coefficients A and B for the indolene mixture. In order to mix indolene with ethanol and express the non-ideal behaviour of the final alcohol-hydrocarbon blends, the vapour pressures will be calculated with a modified Rault's Law with a Wilson model, whose parameters are adjusted to match experimental data. The Wilson model is described in the following section.

2.2 Vapour Pressure

The fugacity is used to calculate the saturation, or vapour, pressure of each component in the blend

$$\ln\ \overline{\varphi}_i = \ln\frac{f_i}{x_i P} = \frac{b_i}{b_m}(Z-1) - \ln(Z-B) - \frac{A}{2\sqrt{2}B}\left(\frac{2\sum_j x_j a_{jk}}{a_m} - \frac{b_k}{b_m}\right)\ln\left(\frac{Z+2.414B}{Z-0.414B}\right) \qquad (7)$$

In this equation the term a_{jk} can be expressed by

$$a_{jk} = \sqrt{a_j a_k}\left(1 - k_{jk}\right) \qquad (8)$$

again, the binary interaction parameter was set to zero as no interaction is considered at this step. For each component at a given temperature, the pressure at which the fugacity of its liquid phase equals the fugacity of its vapour phase represents the component's saturation pressure in the blend.

$$f_i^L = f_i^V \qquad (9)$$

In fact, the deviation from ideality in the calculation of the mixture vapour pressure was assessed by a Rault's law modified with a Wilson model. According to this method, the vapour pressure of the blend is computed as the sum of the partial contributions of each component

$$P_{sat,mix} = \sum_{i=1}^{2} x_i \gamma_i P_{sat,i} \qquad (10)$$

where x_i is the molar fraction and γ_i the activity coefficient of the *i*-component. The activity coefficients were obtained with the Wilson model which, as starting point, expresses the excess Gibbs free energy as function of binary parameters $\Lambda_{i,j}$

$$\frac{g^E}{RT} = -\sum_i x_i \ln\left(\sum_j x_j \Lambda_{ij}\right) \qquad (11)$$

where

$$\Lambda_{ij} = \frac{v_j^L}{v_i^L} \exp\left[-\left(\lambda_{ij} - \lambda_{ii}\right)/RT\right] \qquad (12)$$

the energy parameters for many couple of hydrocarbons (λ_{ij}- λ_{ii}) can be obtained from literature [15] and, technically, the molar volumes v_i, v_j can be substituted by the corresponding parameters 'b' of the components [16] with minor loss of accuracy. In this work, indolene was treated as a pre-mixed surrogate similar to gasoline thus only two Wilson parameters $\Lambda_{1,2} = 0.1615$ and $\Lambda_{2,1} = 0.3527$ for the gasoline/ethanol mixtures were needed and were obtained from the work of Pumphrey et al. [17]. The activity coefficients for the binary system so obtained can be expressed as function of the molar fractions of the constituents

$$\ln(\gamma_1) = -\ln(x_1 + \Lambda_{1,2} x_2) + x_2\left(\frac{\Lambda_{1,2}}{x_1 + \Lambda_{1,2} x_2} - \frac{\Lambda_{2,1}}{x_2 + \Lambda_{2,1} x_1}\right) \qquad (13)$$

$$\ln(\gamma_2) = -\ln(x_2 + \Lambda_{2,1} x_1) - x_1\left(\frac{\Lambda_{1,2}}{x_1 + \Lambda_{1,2} x_2} - \frac{\Lambda_{2,1}}{x_2 + \Lambda_{2,1} x_1}\right) \qquad (14)$$

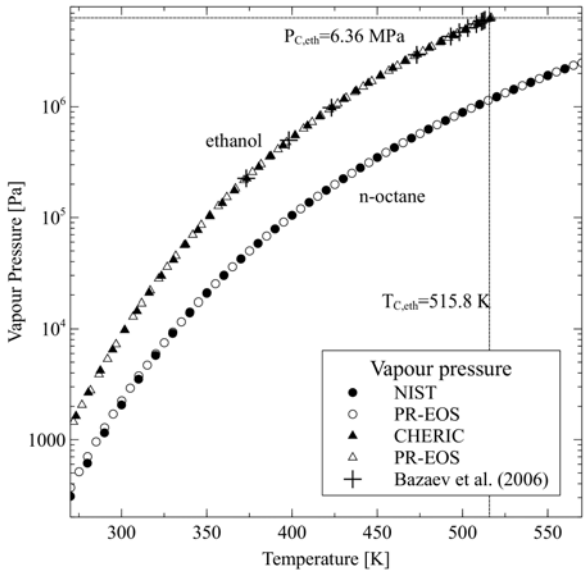

Figure 1: Calculation of vapour pressures for n-octane and ethanol obtained with the PR-EOS and comparison with reference data from literature Refs. [12][18].

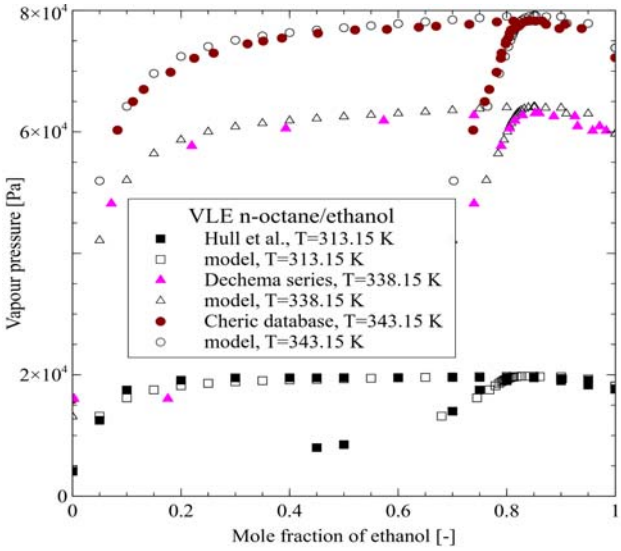

Figure 2: VLE phase diagrams for the binary mixture n-octane/ethanol at different temperatures; values are compared to reference data from literature Refs. [12][19][20].

Finally, the saturation pressure of the non-ideal blend can be obtained using equation (10). Figure 1 shows the comparison between the vapour pressure for n-octane and ethanol calculated with equations (7)-(9) and the values extracted from technical literature [18][12]; the results of vapour-liquid equilibrium (VLE) calculations carried out with the non-ideal model, based on equations (10)(13)(14), are shown in figure 2; the Wilson coefficients used for this calculation were $\Lambda_{1,2} = 0.1290$ and

$\Lambda_{2,1} = 0.1785$ obtained from Ref.[19]; in figure 2, values of bubble point (higher) pressures and dew point (lower) pressures are compared to reference data from Refs. [12] [20] [19]. It is important to point out that the presence of the Wilson coefficients does not affect the calculation of vapour pressure for single species; as a matter of fact, for a mixture 0% indolene and 100% ethanol (x_1=0, x_2=1), equation (14) provides that ln γ_2 =0, thus γ_2 is unity. The ln γ_1 would be non zero, however the mole fraction of indolene x_1 will be zero, therefore giving a null contribution from equation (10). The prediction in this case would be calculated by the simple PR-EOS.

2.3 Reid Vapour Pressure

The common test for evaluating the evaporative characteristics of petroleum fuels is the RVP test defined by the American Society for Testing and Materials under the designation ASTM D323-56. Reid vapour pressure differs from the true vapour pressure (TVP) of a blend, but it is a well documented properties of gasolines, and it is fundamental for the synthesis of the fuel surrogates.

Ref. [21] proposes a correlation between the true vapour pressure and the Reid vapour pressure

$$TVP = \exp\left[E - \left(\frac{F}{T_{LA}}\right)\right] \qquad (15)$$

where TVP is in psia, T_{LA} is the daily average surface temperature of the liquid stock in ° R, while E and F are parameters defined as follow:

$$E = 15.64 - 1.854S^{0.5} - \left(0.8742 - 0.3280S^{0.5}\right)\cdot \ln(RVP) \qquad (16)$$

$$F = 8742 - 1042S^{0.5} - \left(1049 - 179.4S^{0.5}\right)\cdot \ln(RVP) \qquad (17)$$

RVP is the Reid vapour pressure in psia and S is the stock ASTM distillation slope at 10 volume percent evaporated, in degrees Fahrenheit per percent, that can be found in Ref. [21]. In the absence of distillation data, the same document proposes the following values: motor gasoline S=3.0, aviation gasoline S=2.0, light naphtha (RVP 9-14 psi) 3.5, naphtha (RVP of 2-8 psi) S=2.5.

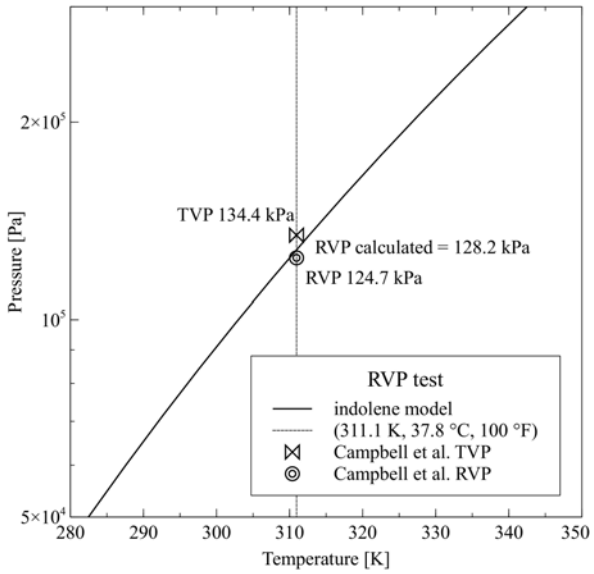

Figure 3: comparison of the RVP reported by Ref. [22] and the RVP calculated by the present model.

In our case, since the TVP is calculated with the PR-EOS, the equation (15) must be solved indirectly, through parameter E, after substituting parameter F (vice-versa is also possible), leading to the relations:

$$RVP = \exp\left[\frac{c_1 - E}{c_2}\right] \qquad (18)$$

$$E = \left(\frac{Tc_2}{Tc_2 - c_4}\right)\left(\ln TVP + \frac{c_3}{T} - \frac{c_4 c_1}{Tc_2}\right) \qquad (19)$$

where

$c_1 = 15.64 - 1.854S^{0.5}$, $c_2 = 0.8742 - 0.3280S^{0.5}$, $c_3 = 8742 - 1042S^{0.5}$, $c_4 = 1049 - 179.4S^{0.5}$

Figure 3 shows a validation test carried out against data published by Campbell [22], who provided the RVP value of a hydrocarbon mixture whose composition is shown in Table 1.

He reported an RVP of 124.7 kPa (18 psi) and a TVP of 134.4 kPa (19.5 psi). The RVP calculated with the present model, for the same blend, was 128.2 kPa, in good agreement with the results of Ref. [22].

Component	Mole fractions in Ref.[22]	Boiling point [K]	Tc [K]	Pc [bar]	Vc [m3/kg kmol] e-4	Zc [-]	Acentric factor ω [–]	Mol. weight [kg/mol]
I-Butane (b)	9.14	262.2	407.8	36.04	2.590	0.275	0.183	58.12
N-Butane (a)	17.10	272.6	425.12	37.96	2.550	0.274	0.199	58.12
I-Pentane (b)	9.09	309.0	469.8	33.70	3.060	0.272	0.250	72.15
n-Pentane (a)	6.02	300.9	461.0	33.81	3.060	0.272	0.229	72.15
N-Hexane (a)	16.84	341.9	507.6	30.25	3.680	0.264	0.299	86.17
N-Heptane (a)	41.81	371.56	540.10	27.40	4.281	0.262	0.349	100.20

Critical and reference properties obtained from: ([a]) Ref.[18]; ([b]) = Ref.[12]

Table 1: composition used by Ref. [22] for the RVP and for calculation reported in figure 3, and critical parameters of single component.

2.4 Density

Densities are directly calculated from the PR-EOS, by relating the vapour pressure and the compressibility Z. By solving eq. (4) for minimum and maximum compressibility, the densities are calculated as

$$\rho_{gas} = \frac{P_{sat} M_W}{Z_{max} RT} \quad \text{and} \quad \rho_{liq} = \frac{P_{sat} M_W}{Z_{min} RT} \qquad (20)$$

Over the critical point $Z_{max}=Z_{min}$ thus one only solution is calculated by the PR-EOS.

2.5 Enthalpy

The enthalpy departure function was here used to calculate the difference between the real fluid enthalpy and the ideal gas enthalpy (identified by a star superscript):

$$h - h^* = RT(Z-1) + \frac{T\frac{da}{dT} - a_m}{2\sqrt{2}b_m} \ln\left(\frac{Z + 2.414B}{Z - 0.414B}\right) \qquad (21)$$

The ideal molar enthalpy was calculated as a function of the temperature by using a polynomial function as proposed by McBride et al. [5]

$$\frac{h^*}{RT} = a_1 + \frac{1}{2}a_2 T + \frac{1}{3}a_3 T^2 + \frac{1}{4}a_4 T^3 + \frac{1}{5}a_5 T^4 + \frac{b_1}{T} \qquad (22)$$

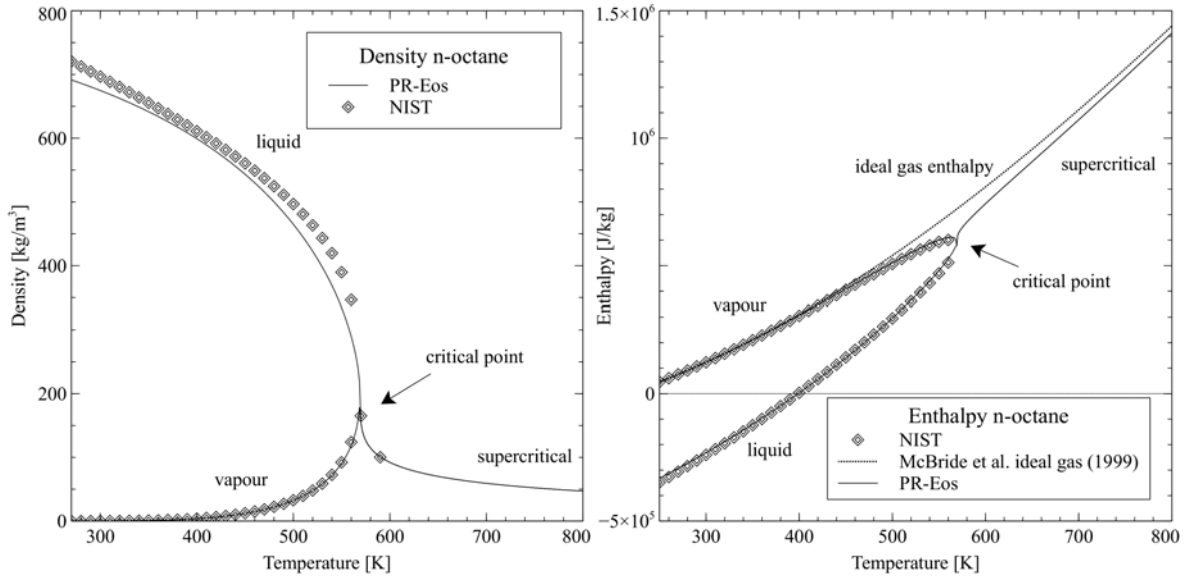

Figure 4: comparison of the densities and enthalpies for n-octane reported by Ref. [18] and the densities and enthalpies calculated by the present PR-EOS based model.

The enthalpy is first calculated at the boiling point temperature and then this value is subtracted from the enthalpy calculated at the local temperature. The coefficients for the polynomial relation for the implemented species can be found in the work of Ref. [5].

2.6 Specific Heat Capacity

Constant pressure specific heat capacities were obtained, for each blend, by the thermodynamic relation

$$C_P(p,T) = \left(\frac{\partial h}{\partial T}\right)_P - \frac{1}{dT}\left[v - T\left(\frac{\partial v}{\partial T}\right)_p\right]dp \qquad (23)$$

where the partial derivative of specific volume with respect of temperature can be expressed, using the PR-EOS, by

$$\left(\frac{\partial v}{\partial T}\right)_p = \frac{R}{p}\left[\left(\frac{\partial Z}{\partial T}\right)_p T + Z\right] \qquad (24)$$

and

$$\left(\frac{\partial Z}{\partial T}\right)_p = \frac{-Z^2\frac{\partial B}{\partial T}|_p + Z\left(6B\frac{\partial B}{\partial T}|_p + 2\frac{\partial B}{\partial T}|_p - \frac{\partial A}{\partial T}|_p\right) + B\frac{\partial A}{\partial T}|_p + \left(A - 2B - 3B^2\right)\frac{\partial B}{\partial T}|_p}{3Z^2 + 2(B-1)Z + A - 3B^2 - 2B} \qquad (25)$$

with $$\frac{\partial B}{\partial T}|_p = \frac{-bp}{RT^2} \text{ and } \frac{\partial A}{\partial T}|_p = \frac{p}{R^2T^2}\left(\frac{da}{dT} - \frac{2a}{T}\right) \quad (26)$$

$$\frac{da}{dT} = \frac{-a_c k}{2\sqrt{TT_c}}\left[1 + k\left(1 - \sqrt{\frac{T}{T_c}}\right)\right] \quad (27)$$

The term $\left(\frac{\partial h}{\partial T}\right)_P$ was evaluated numerically, although an analytical derivation from equation (21) is also possible. The constant volume specific heat capacity was obtained with the thermodynamic relation

$$C_V(p,T) = C_p(p,T) + \frac{T}{\rho^2}\left(\frac{\partial \rho}{\partial T}\right)_p \left(\frac{\partial p}{\partial T}\right)_\rho - p\left(\frac{\partial v}{\partial T}\right)_p \quad (28)$$

where

$$\left(\frac{\partial p}{\partial T}\right)_\rho = \left(\frac{\partial p}{\partial T}\right)_v = \frac{R}{v+b} - \left(\frac{da}{dT}\right)_v \frac{1}{v^2 + 2vb - b^2} \quad (29)$$

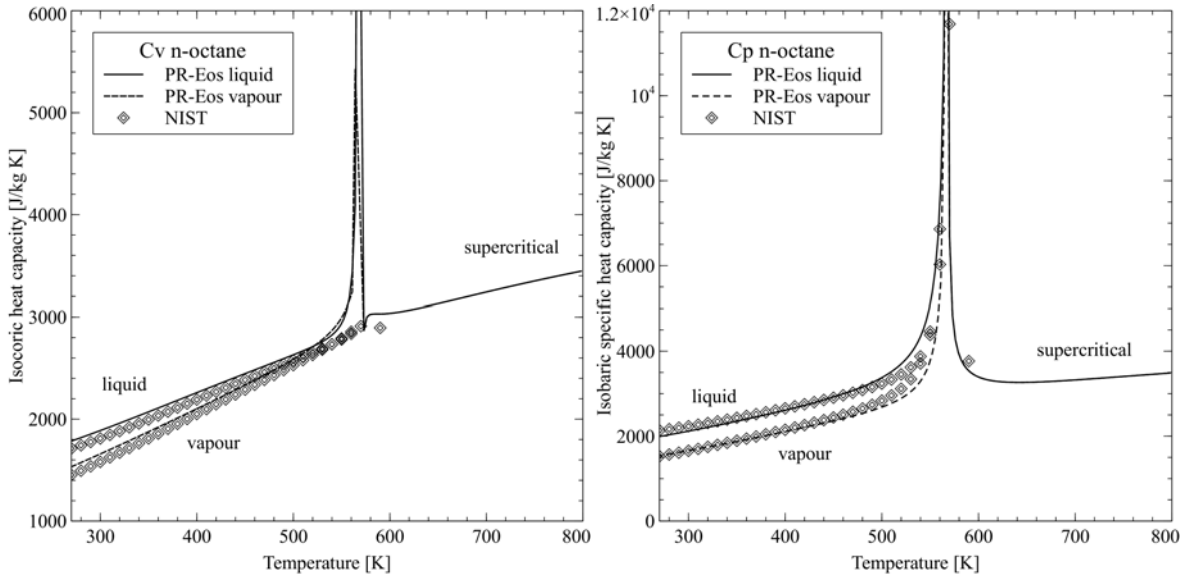

Figure 5: comparison of the isobaric and isocoric specific heat capacities for n-octane reported by Ref.[18] and the calculated by the present PR-EOS based model.

and, finally, the partial derivative of density with respect of temperature expressed by

$$\left(\frac{\partial \rho}{\partial T}\right)_p = -\rho^2\left(\frac{\partial v}{\partial T}\right)_p = \frac{-\rho^2 R}{p}\left[\left(\frac{\partial Z}{\partial T}\right)_p T + Z\right] \quad (30)$$

Near the critical point, the divergence of some thermodynamic properties related to compressibility,

among which the isobaric heat capacity C_P, is a well known fact since the first appearance of the 'van der Waals' cubic equation of state in 1872. This phenomenon can be described by the PR-EOS, and the calculations were supported by the data extracted from the NIST database. Discontinuity in the isochoric heat capacity C_V, is also documented in literature Ref. [23] although this behaviour was not emerging from NIST's data set. It is also well known the flattening effect that an increase in pressure has on the peaks of these curves. The extent to which the peak will expand in real fluids would probably be limited and complicated by the effects of gravity as well, thing that it is not considered in the present modelling. In equation (28), the second and the third terms on the right side of the equation, which represent respectively the work done against intermolecular attraction of the substance itself and the work done against the environment in isobaric heating, have the same sign (it can be can proved by substituting equation (30)) and certainly counterbalance the divergence of the first term, C_P. However, a sensitivity analysis of these 'anomalies' of fluids with respect of pressure is beyond the scope of the present work, and the values predicted by the PR-EOS at critical point were moderated by numerical interpolation to get around the discontinuity.

2.7 Entropy

Entropy was obtained from the specific heat through the following thermodynamic relations [24]

$$ds = \frac{c_P}{T} dT - \left(\frac{\partial v}{\partial T}\right)_P dp \qquad (31)$$

which for an ideal gas reads

$\Delta s = s^* - s_{ref} = \int \frac{c_P}{T} dT - R\ln\frac{p_2}{p_1}$, where Sref=0 for the liquid phase at boiling point (normal boiling point convention). Obtaining the ideal entropy from the specific heat capacity was particularly convenient as avoided the necessity of implementing a dedicated function for ideal entropy with all the coefficients that would have been required for each species by a polynomial function like done for enthalpy. After obtaining the entropy function for the ideal gases, a departure function for entropy, derived from the Peng-Robinson equation of state, was used to calculate the entropy of liquid, vapour and supercritical phases:

$$s(T,p) - s^* = R\ln(Z-B) + \frac{\frac{da}{dT}}{2\sqrt{2}b_m}\ln\left[\frac{Z+\left(1+\sqrt{2}\right)B}{Z-\left(1-\sqrt{2}\right)B}\right] \qquad (32)$$

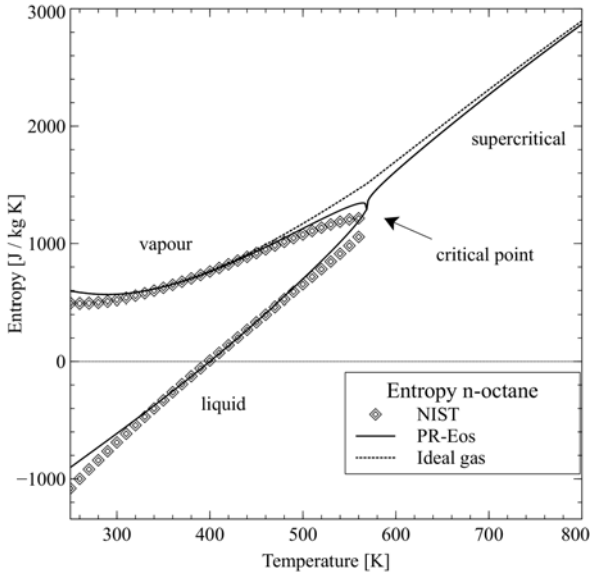

Figure 6: comparison of entropy for n-octane reported by Ref. [18] and calculated by the present PR-EOS based model.

2.8 Viscosity

Based on the similarity of PvT and TμP relationships, a PT viscosity equation was derived from the PR-EOS equation of state. The development of EOS based model for viscosity, first appearing in the work of Phillips [25] in 1912; in 1997, Guo et al. [26] proposed a PR-EOS based viscosity model. EOS based viscosity models gained popularity in the last decades among reservoir and process simulations and calculations. The main reason beside their success versus empirical correlations lays in the improved thermodynamic consistency between the transport and the equilibrium properties. In fact, the viscosity of both gas and liquid phases can be described by a single model, achieving a smooth transition near and across the critical point.

The PT-μ model implemented here was proposed by Ref. [14]. As in other EOS based models, the derivation of the viscosity equation was obtained by interchanging the positions of T and P in the PR EOS and by replacing the specific volume *v* with the viscosity μ, and the gas constant R with a parameter R', subsequently defined. Eq. (1) was then transformed into the following:

$$T' = \frac{Rp}{\mu - b} - \frac{a(T)}{\mu^2 + 2\mu b - b^2} \qquad (33)$$

where a pseudo-temperature T' was introduced to correct the calculated viscosities based on best fit of experimental data $T' = T - T_d$, $T_d = 0.45\ T_c$.

In this viscosity model, P denotes pressure, bar; T the temperature, K; μ the viscosity, 10^{-7} Pa s and the subscript c refers to critical state. Solving the PT-μ equation at the critical point renders

$$a = 0.45724 \frac{r_c^2 P_c^2}{T'_c} \qquad (34)$$

$$b = 0.0778 \frac{r_c P_c}{T'_c} \qquad (35)$$

$$Z_c = \frac{T'_c \mu_c}{r_c P_c} = 0.3074 \qquad (36)$$

from which

$$r_c = \frac{T'_c \mu_c}{0.3074 P_c} \qquad (37)$$

The critical viscosity μ_c was calculated from the empirical correlation of μ_c with critical temperature T_c, critical pressure P_c and molecular mass M_w:

$$\mu_c = 7.7 T_c^{-1/6} M_w^{1/2} P_C^{2/3} \qquad (38)$$

where μ_c is in micropoise (1 uP=10^{-7} Pa s). The parameter R' is defined as followed

$$R' = \beta(P) r_c \qquad (39)$$

$$\beta(P) = e_0 \left(1 - P_r^{-1}\right) - 0.02715 P_r^{-1} \left[(P_r + 0.25)^{-1} - 0.8\right] + P_r^{-1} \qquad (40)$$

$$P_r = \frac{P}{P_c} \qquad (41)$$

The coefficient e_0 is a function of molecular mass M_w and acentric factor ω:

$$e_0 = 0.03192 - 3.3125 \times 10^{-4} M_w \omega \qquad (42)$$

The above viscosity model developed from PR EOS has been used by many authors [14] [26] with good results. Equation (33) can also be expressed in terms of compressibility factor by using, in analogy with PR-EOS, a generalized equation for viscosity of the kind

$$T' \mu = Z R' P \qquad (43)$$

In this case, by settings $Z = \frac{T' \mu}{R' P}$, $Z = \frac{T' \mu}{R' P}$, $A = \frac{a T'}{R'^2 P^2}$, the PT-μ equation becomes cubic in Z

$$Z^3 - Z^2(1-B) + Z\left(A - 3B^2 - B\right) - \left(AB - B^2 - B^3\right) = 0 \qquad (44)$$

and it can be solved by the same numerical algorithm implemented in the PR cubic eos. However, the values of the constants A, B, a, b and, therefore, the values of Z are different from the one defined for the PvT equation of state in section 2.1.

The saturation domain is, in analogy with the PR-EOS, characterized by three real distinct solutions for Z and, obviously for μ, of which, in contrast to the PR-EOS, the smallest value represents the viscosity of vapour phase and the largest value represent the viscosity of the liquid phase. The intermediate solution must be discarded as it does not have any physical meaning. Calculations of μ over the critical pressure and temperature can be performed, giving values of viscosity for supercritical fluids. In this latter case only one real root is calculated.

To improve accuracy in the calculations, especially for the liquid phase, a correction of viscosity was introduced as suggested by Ref. [14]; the corrective model employed is based on the addition of two extra terms to the one obtained by the PT-μ model:

$$\mu = \mu^{PR} + c_0 + c \qquad (45)$$

Where μ^{PR} is the viscosity calculated from Eq. (33), c_0 is expressed as a function depending on P_r which satisfy $c_0 = 0$ while $P_r = 1$:

$$c_0 = 6.714(P_r - 1) - 127.8\left[(P_r + 1)^{-1} - 0.5\right] \qquad (46)$$

and c has different correlations for vapour and liquid phases.

Correction of liquid viscosity

Parameter *c* is dependent on μ^{PR} calculated from Eq. (33) which satisfy c = 0 while $\mu_r = 1$, where

$$\mu_r = \frac{\mu^{PR}}{\mu_c} \qquad (47)$$

$$c = e_3 \ln\mu_r + e_4(\mu_r - 1) + e_5\left[(\mu_r + 1.25)^{-1} - 0.4444\right] \quad \mu_r > 1 \qquad (48)$$

and for the gas phase is as following:

$$c = 3000\ln\mu_r + e_1(\mu_r - 1) + e_2\left[(\mu_r - e_6)^{-1} - (1 - e_6)^{-1}\right], \quad \mu_r \le 1 \qquad (49)$$

The coefficients e_1,_,e_6 are functions of the acentric factor ω and were derived and reported in the work

of Ref.[14]. The congruence of the results was obtained by imposing that the two correction terms c, for liquid and gas phase, should have the same derivative at $\mu_r = 1$, $\left(\frac{\partial c}{\partial \mu_r}\right)_{\mu_r=1}$.

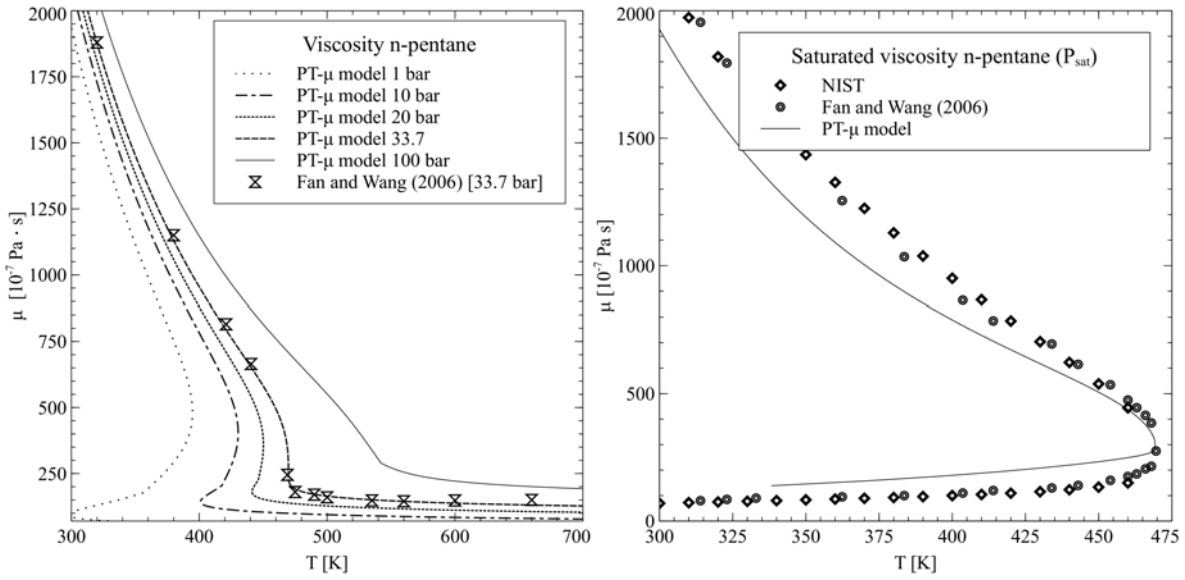

Figure 7: comparison of saturated (Psat) and supercritical viscosity for n-pentane reported by Ref. [18] and calculated by the implemented PT-μ model.

In the subcritical region, the saturated liquid and vapour viscosities depend on temperature and the saturation pressure; the saturation vapour pressure was calculated with the PR-EOS. Figure 7 shows that the implementation of the viscosity model was done correctly.

2.9 Surface tension

The calculation was performed following two different methods, on the base of the working fluid. The first method implemented, proposed by Sastri et Rao [10] is accurate for alcohols:

$$\sigma = K\left(\frac{P_C}{10^5}\right)^x (T_{bo})^y (T_C)^z + \left(\frac{1-T_r}{1-\frac{T_{bo}}{T_C}}\right)^m \qquad (50)$$

The factor 10e5 is needed to enter the pressure in Pa. The constants are

$$K = 2.28 \;\; x = 0.25 \;\; y = 0.175 \;\; z = 0. \;\; m = 0.8 \qquad (51)$$

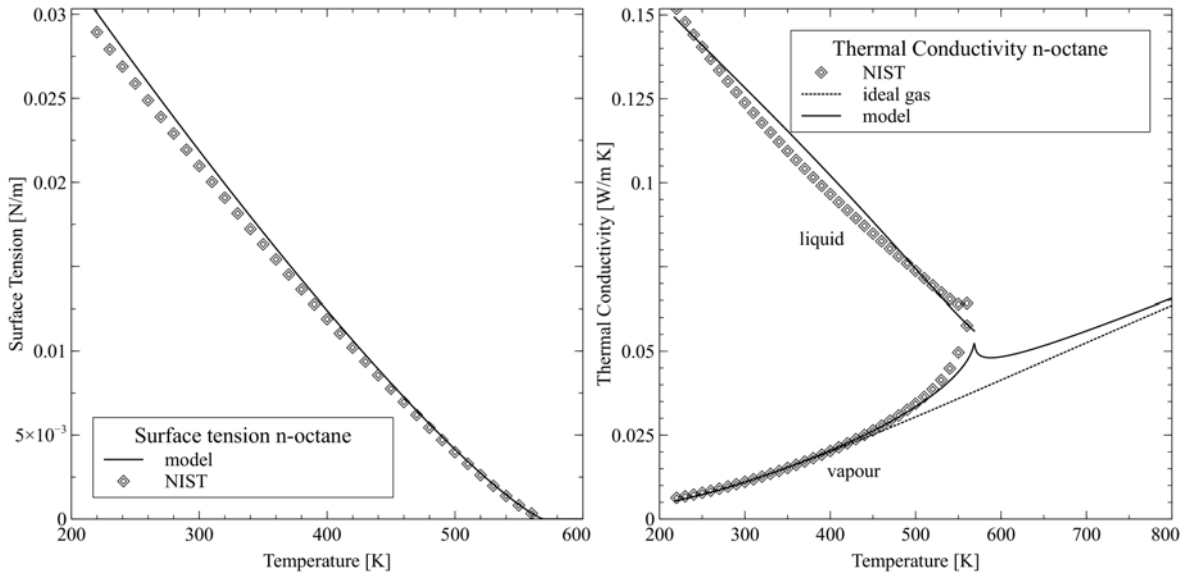

Figure 8: comparison between surface tension and thermal conductivity for n-octane reported by Ref.[18] and calculated by the implemented model.

The second method selected was the one proposed by Pitzer [11], which produces accurate results with hydrocarbons

$$\sigma = \left(\frac{P_C}{10^5}\right)^{2/3} T_C^{1/3}\left(1.86+\frac{1.18\omega}{19.05}\right)\left(\frac{3.75+0.91\omega}{0.291-0.08\omega}\right)^{2/3}(1-T_r)^{\frac{11}{9}} \qquad (52)$$

where omega is the acentric factor.

2.10 Thermal Conductivity

Thermal conductivity of both liquid and vapour was calculated by using a multi-step procedure. The first step calculated the thermal conductivity of an ideal gas using a polynomial relation

$$\log\lambda(i) = C_1 logT + \frac{C_2}{T} + \frac{C_3}{T^2} + C_4 \qquad (53)$$

The values of the constants C_1 - C_4 were found in the work of Ref [5].

The quantity λ was calculated for every component of the blend and then the ideal gas blend's thermal conductivity was obtained by averaging over molar fractions

$$\lambda_{blend} = \sum x_i \lambda_i \qquad (54)$$

This formula is quite popular but it does not account for the effects of compressibility, in the saturation

region. In the present work, a new formulation was adopted for real gases, which was validated against NIST values for octane, dodecane and heptane. The validation versus n-octane is shown in figure 8. This formulation attempts to consider the effects of compressibility and gives a smooth transition through the critical point and consistency with the thermodynamic data calculated with the PR-EOS:

$$\lambda_V = \lambda_{blend}\left(1 + 0.35 \cdot \log\frac{1}{Z_{max}}\right) \qquad (55)$$

The values of λ_{crit} were found applying equation (54) at the critical point, while the coefficient 0.35 was found by fitting data from Ref. [18]. As for the liquid phase an expressions proposed by Latini et al. [13] was implemented. This equation reads

$$\lambda_L = A\frac{(1-T_r)^{0.38}}{T_r^{0.167}} \qquad (56)$$

where A is expressed by

$$A = \frac{A^* \cdot \sigma_b^{\alpha}}{M_w^{\beta} \cdot T_C^{\gamma}} \qquad (57)$$

where α=1.2, β=0.5, and γ=0.167.

The value of the constant A^* depends on the species. In the present model three different values were considered, $A^* = 0.00350$ for hydrocarbons, $A^* = 0.00339$ for alcohols, and $A^* = 0.494$ for other compounds, as suggested by Ref. [13]. This correlation works properly within the middle range, which is above the triple point and below the critical point, and is equal to zero at critical. The real behaviour of thermal conductivity of a liquid is different in the way it is not zero at the critical point and has a more linear trend linking the triple point to the critical point. To account for this deviation from real behaviour, in this work the Latini's formulation is blended with a linear correlation, which force the thermal conductivity equation to respect both the critical point and the triple point, becoming consistent with the predictions of equation (55) for the vapour phase.

In order to do this a linear function was defined, with boundary conditions and, which resulted into:

$$\lambda(T) = \lambda_3 + \left(\frac{\lambda_C - \lambda_3}{T_3 - T_C}\right)(T_3 - T) \qquad (58)$$

Now, while λ_C can be obtained from equations (53) and (54) applied at the critical point, the value of λ_3

was unknown. To calculate λ_3 , at the triple point, a reference value of λ was obtained by averaging thermal conductivity of high, medium and low boiling point hydrocarbons, dodecane, n-octane, and n-heptane, at a reference temperature sufficiently below the minimum value of temperatures needed for this study, T_{ref}=220 K. This reference value, 0.153 W/m K, was used to build the linear correlation for thermal conductivity in a reduced reference frame, somewhat in analogy with the principle of corresponding states, as follow

$$\lambda_3 = 0.153(1 + \Delta T_{3r}) \qquad (59)$$

where $\Delta T_{3r} = (T_{3,r} - T_{ref,r})$, $T_{ref,r} = \frac{220}{T_C}$ and $T_{3,r} = \frac{T_3}{T_C}$ and the reduced triple temperature of the blend was calculated

$$\lambda_{3,blend} = \sum x_i \lambda_{3,i} \qquad (60)$$

Finally, a blending function connects Latini's equation with the linear correlation eq. (58), correcting the difformities from the real behaviour

$$\lambda_{L,corr} = \left(1 - \frac{T}{T_C}\right)\lambda_L + \left(\frac{T}{T_C}\right)\lambda_{linear} \qquad (61)$$

Improvement can be brought in the future by extending the prediction of λ_3 to a larger group of reference substances, but the results were considered satisfactory for this application.

3. Synthesis of the surrogate biofuels

3.1 Distillation Curves

The distillation characteristics are critically important for both automotive and aviation gasolines performances, affecting starting, warm-up, and tendency to vapour-lock at high operating temperature or at high altitude, or both. The presence of high boiling point components in these and other fuels can significantly affect the degree of formation of solid combustion deposits. The distillation characteristics of hydrocarbons have an important effect also on their safety. The boiling range gives information on the composition, the properties, and the behaviour of the fuel during storage and use.
Distillation limits are often included in petroleum product specifications, and distillation curves are normed by regulation, for example ASTM D86 [27] in the United States. In this procedure, 100 ml of fuel are heated and 4 ml of fuel vapours are collected every minute in a condenser. As a result, the fuel vapour temperature can be correlated with the fraction of fuel evaporated. Theoretically, the shape of the resulting curve is a characteristic of any particular fuel. However, the composition of a commercial

fuel shows some variability instead from batch to batch.

The ASTM distillation procedure was here simulated by calculating the number of moles of each component in the vapour phase at different temperatures, considering a closed volume at constant atmospheric pressure. The calculations were performed by using the Rachford-Rice equation.

During distillation, the composition of the liquid and vapour phases change at different temperatures, because more volatile components vaporize first, while the heavier components vaporize at last. In order to understand whether a fuel surrogate properly represented the volatility characteristic of the real fuel, the simulation of the ASTM distillation test and the RVP test of the fuel model were compared to experimental data.

The Rachford-Rice flash equation solves flash calculations where T and P are known; this calculation often refers to **pT-flash**. RR-equation is, for an ideal mixture, a function of molar fractions of feed F, the coefficient K_i=Psat(i)/P and the vapour fraction V/F. Using conservation of mass for liquid and vapour phases then the molar compositions of each component in the liquid and vapour phase can be calculated:

$$\sum \frac{z_i(K_i - 1)}{1 + \frac{V}{F}(K_i - 1)} = 0 \qquad (62)$$

A physical solution must satisfy $0 \leq V/F \leq 1$. The Newton-Raphson numerical method was used to calculate the vapour fraction in the Rachford-Rice equation. The Newton's method estimates a better root using the last guess and the ratio of the function and its derivative calculated at the same point; setting a_i=V/F, the function and its first derivative are:

$$f(a_i) = \sum \frac{z_i(K_i - 1)}{1 + a_i(K_i - 1)} \qquad (63)$$

and

$$f'(a_i) = \sum \frac{z_i(K_i - 1)^2}{(1 + a_i(K_i - 1))^2} \qquad (64)$$

To solve the RR-equation we solved for a_i:

$$a_{i+1} = a_i - \frac{f(a_i)}{f'(a_i)} \qquad (65)$$

which takes the explicit form

$$f(a_{i+1}) = f(a_i) + \frac{\sum \frac{z_i(K_i - 1)}{1 + a_i(K_i - 1)}}{\sum \frac{z_i(K_i - 1)^2}{(1 + a_i(K_i - 1))^2}} \qquad (66)$$

where z is the mole fraction of component i and K is given as

$$K = \frac{\gamma_i P_{sat}^i}{P} \qquad (67)$$

where γ_i and P_{sat} are the activity coefficient and saturation pressure of the component -*i* respectively and P is the pressure in the system. Eq. (63) is non linear and in order to guarantee the convergence of the Newton's method the value of *a* was bracketed within the range [0,1].

3.2 Ethanol fuel blends

Ethanol C2H5OH (or CH3CH2OH) is an alcohol which molecular structure shows a polar fraction, due to the -OH radical, and a non polar fraction in its carbon chain. As a consequence, ethanol can be dissolved in both gasoline (non polar) and in water (polar), although the non polar properties prevail due to its short carbon chain. From one side, ethanol's polar characteristics result in a highly hygroscopic behaviour, which means that ethanol tends to attract water. Hydrous ethanol has a water content that ranges from 4% to 7% by volume and can be produced by simple distillation. Dehydration is instead required to obtain anhydrous ethanol, with a water content lower than 1.0 %.

In common ethanol-gasoline blends in use today, water is usually removed to the extent possible to avoid phase separation in fuel handling, storage, and distribution equipment. Therefore only anhydrous ethanol is considered in this study. It should also be noted that up to 2% denaturant is added to ethanol prior to gasoline blending, which makes the actual content of ethanol lower than the quantity declared; for example there is up to 83% in volume of ethanol in E85 and roughly 13% ethanol in E15. The content may also be subject to seasonal variations to adjust the fuel's volatility.

The formation of hydrogen bonds in ethanol molecule results in higher boiling temperature in

comparison to that of gasoline. This is confirmed by the fact that ethanol forms azeotropic mixtures with the gasoline hydrocarbons at around 10-15% concentrations, greatly impacting the fuel blend's volatility, which results substantially greater than expected for ideal mixtures. In this work, this aspect will be considered when modelling the vapour pressures by using activity coefficients. On a final note, since the hydrocarbon components used to model the certification fuel in this work are usually present in commercial gasoline, we will assume that the modelled certification fuel here will behave not differently from gasoline in terms of phase equilibrium when mixed with ethanol. Furthermore, phase separation only occurs at relatively high concentrations of water and should not be of concern when using anhydrous ethanol.

3.3 The surrogate biofuels

Experimental and simulated engine testing are complicated by the large variability of components in the gasoline available at the pumps, which makes it very difficult to correlate the numerous factors with congruent conclusions during experiments. In this perspective, certification fuel certainly makes things easier, being free from the batch to batch variability to which real gasoline is, instead, subject to. To complicate things even further, must be added the fact that most of the thermophysical properties of real fuels are not published and not well known.

Two main characteristics were considered as major drivers for the creation of the fuel surrogates, both related to fuel volatility: the *distillation curve* and the *vapour pressure*. Validations was taken against these two properties for the multi-component fuels.

The distillation characteristics are critically important for automotive gasoline performances, affecting starting, warm-up, and tendency to vapour lock at high operating temperature. Distillation limits are often included in petroleum product specifications, and distillation procedures are established by regulation, Ref. [27].

Vapour pressure also plays a very important role in the phase change of the fuel, especially when mixture of gasoline and ethanol are involved. The tendency to vaporize of some gasoline-alcohol blends is notoriously higher than the volatility of either pure gasoline or ethanol. This behaviour is said to be non-ideal, because it shows a non linear behaviour and depends on the reciprocal concentrations of components. The activity coefficients, calculated with eq. (12) (13), were used to model the variation of the blend's vapour pressure with respect to the alcohol concentration, making the numerical simulation physically more realistic.

The work of Andersen et al. [28][29] provided an excellent experimental framework to which

comparing distillation and volatility results and on which constructing the fuel surrogates needed for the numerical calculations. In their work they used a base gasoline without additives, Haltermann EEE, similar to "Indolene" from Amoco/BP, the one used in the US Federal Test Procedure (FTP) to certify vehicles for compliance with emissions regulations, and they performed experimental measurements of RVP [28] and distillation curves [29] for this certification fuel and its blends with ethanol and other alcohols. They reported the EEE gasoline Reid vapour pressure to be of 60-63 kPa (8.7-9.1 psi). Since Andersen et al. did not reported the exact composition of the certification fuel adopted in their work, a further reference for modelling of the certification fuel was found in Greenfield et al. [30]. Ref.[30] presented distillation calculations using two surrogate models, one for a certification fuel similar to indolene, and one for an oxygenated mixture, both compositions are shown in table 2:

Fuel	NC4	IC5	EtOH	C6	iC8/nC8	Tol	124 TMB	nC13
Certification	5	13	0	3	31	27	19	2
Oxygenated	5.25	23.75	13	10	10	24	12	2

Table 2: compositions used by Ref.[30] to simulate the distillation characteristics of real-like fuels

The surrogate for indolene used in the present work was synthesized on the basis of the certification surrogate proposed by Ref.[30], with minor adjustments to the composition in order to optimize it to the distillation and RVP characteristics presented by Andersen et al [28][29]. These adjustments found justification in the fact that the compounds used in this work do not represent the exact spectrum of compounds of the certification fuel used by Refs.[28][29].

The validation of the surrogate model was taken against both the distillation procedure and the vapour pressure test performed by Refs.[17][26[[27].

Table 3 and 4 provide the compositions and main characteristics of each component used in modelling and of each fuel blend synthesized. The critical parameters as well as the molecular weight, freezing and boiling point temperatures and acentric factor for single species were obtained from literature [18][12]; those ones for the mixtures, shown in table 5, were obtained by averaging the properties of pure components by their mole fraction x_i present in the blend. It is important to recognize the existence of theoretically more accurate methods for calculating critical point of mixtures [31] [32]; however, the work of Jun Cai, Ying Hu, John M. Prausnitz [33] suggests that, for alkane mixtures, the calculation of critical-point parameters used in a cubic EOS can be expressed by a function of the moments of a characterizing quantity, conveniently by *average molecular weight,* which is the first moment of the molecular-weight distribution. This result actually originated from the work of Cotterman et al. (1985) [34]; in calculating the chemical potential of a mixture of heavier paraffins (C_4

- C_{40}), Cotterman et al. found that the parameters $a^{1/2}(T)$ and b of the two constant Soave-Redlich–Kwong (SRK) EOS, which were determined from vapour pressure data, were linear functions of molecular weight. Considering our system, indolene is a mixture of straight or branched single-bonded chain hydrocarbons, well in the range described by Cotterman et al., for which molar fraction averaging should provide reliable results. In order to show the linearity of the implemented mixing method, the calculated coefficients $a^{1/2}(T)$ and b of the PR-EOS are plotted versus the mixture molecular weight in Figure 9.

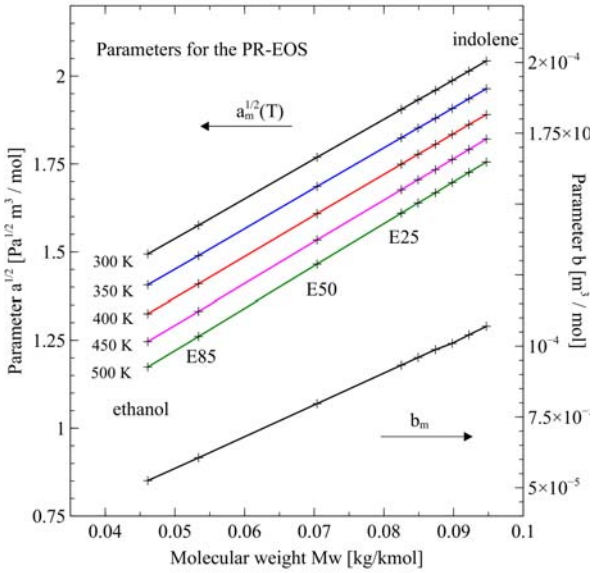

Figure 9: The model used in the present work implies a linear correlation of the square root of the attractive parameter $a_m(T)$ and the repulsive parameter b_m versus the mixture's molecular weight.

When indolene is mixed with ethanol, some deviations from this behaviour might be expected. An appraisal of the extent of these deviations could be done, for example, by introducing interaction parameters in the mixing rules. However, as highlighted by Valderrama [35], the introduction of such parameters does not improve correlations in some complex cases such as in supercritical fluid processes and, therefore, it was not considered in the primary objectives of this work. Finally, when hydrocarbons are mixed with nitrogen, as in the case of air-fuel mixing analysis, a more accurate method should be used as suggested by Michelsen and Heidemann [31] and Peng and Robinson [32]. The results of the distillation predictions obtained with the present model indolene, E5, E10, E15, E20, E25, E50, and E85 are shown in figure 10 and compared to the experimental results provided by Ref. [29].

Comp.	Formula	Mol. weight [kg/mol]	Freezing point [K]	Boiling point [K]	Tc [K]	Pc [bar]	Vc [m3/kg kmol] e-4	Zc [-]	Acentric factor ω [–]
N-butane [(a)]	C4H10	58.12	134.9	272.6	425.1	37.96	2.550	0.274	0.199
2-meth-bu [(a)]	C5H12	72.15	113.3	300.9	461.0	33.81	3.060	0.272	0.229
N-pentane [(a)]	C5H12	72.15	143.0	309.0	469.8	33.70	3.060	0.272	0.250
i-octane [(b)]	C8H18	114.23	165.83	372.3	543.8	25.70	4.680	0.266	0.303
Toluene [(a)]	C7H8	92.14	178.15	383.8	591.7	41.13	3.160	0.264	0.257
123TM-B [(b)]	C9H12	120.19	248.0	449.0	664.5	34.54	3.620	0.265	0.371
n- Tridec [(b)]	C13H28	184.36	268.0	508.6	675.0	16.80	8.230	0.246	0.619
ethanol [(b)]	C2H6O	46.07	159.10	351.45	515.80	63.60	1.680	0.240	0.644

Reference values obtained from: ([a]) Ref.[18]; ([b]) = Ref.[12]

Table 3: main characteristics of the surrogate components used in modelling

The 'kink' appearing in the range 20%-90%, depending on the blend, is a typical non-ideal behaviour of the distillation process due to the disappearing of ethanol within the liquid blend; this 'S-shape' was well captured by the code for all the oxygenated fuel. An evident plateau is shown for the blend E85 in both experimental and numerical data, were about 80% of the blend distilled within a narrow range of temperature close to the boiling point of ethanol.

Comp.	E0	E5	E10	E15	E20	E25	E50	E85
n-butane	0.083	0.079	0.075	0.071	0.066	0.062	0.041	0.012
2-meth-bu	0.207	0.197	0.187	0.176	0.166	0.155	0.103	0.031
n-pentane	0.03	0.028	0.027	0.025	0.024	0.022	0.015	0.004
i-octane	0.2	0.19	0.18	0.17	0.16	0.15	0.1	0.03
toluene	0.335	0.318	0.301	0.285	0.268	0.251	0.167	0.050
123TM-B	0.12	0.114	0.108	0.102	0.096	0.09	0.06	0.018
n- Tridec	0.025	0.024	0.022	0.021	0.02	0.019	0.012	0.004
ethanol	0	0.05	0.1	0.15	0.2	0.25	0.5	0.85

Table 4: compositions of the fuel surrogates used in modelling in mole fractions.

Figure 11 shows isothermal vapour pressure calculation of the indolene surrogate presented here with the activity coefficients calculated using the Wilson model. In particular, the picture shows three calculated lines, the TVP of the surrogate and the RVP of the surrogate with coefficients provided by Pumphrey et al. Ref.[17], the same RVP value of the surrogate with modified Wilson coefficients to match the experimental points, and two sets of experimental points, the one presented by Pumphrey et al., and the one presented by Andersen et al. Ref.[28].

surrogate	Pc [MPa]	Tc [K]	Zc	acentric factor ω	Mol. weight Mw [kg/kmol]	Triple point T [K]	Tboil [K]	RVP [kPa]
indolene	3.46	548.40	0.267	0.280	0.094	168.25	363.54	62.42
E5	3.61	546.77	0.265	0.298	0.092	167.73	362.94	65.46
E10	3.75	545.14	0.264	0.316	0.090	167.22	362.33	66.22
E15	3.89	543.51	0.263	0.335	0.088	166.71	361.73	66.28
E20	4.04	541.88	0.261	0.353	0.085	166.20	361.12	66.11
E25	4.18	540.25	0.244	0.589	0.082	165.69	360.52	65.83
E50	4.91	532.10	0.253	0.462	0.071	163.12	357.50	63.52
E85	5.92	520.70	0.244	0.589	0.053	159.54	353.27	48.20
ethanol ([b])	6.36	515.80	0.240	0.644	0.046	158.00	351.45	15.51

Reference values obtained from: ([b]) = Ref.[12], except RVP.

Table 5: Calculated critical parameters, temperatures and Reid vapour pressure of the fuel surrogates used in modelling.

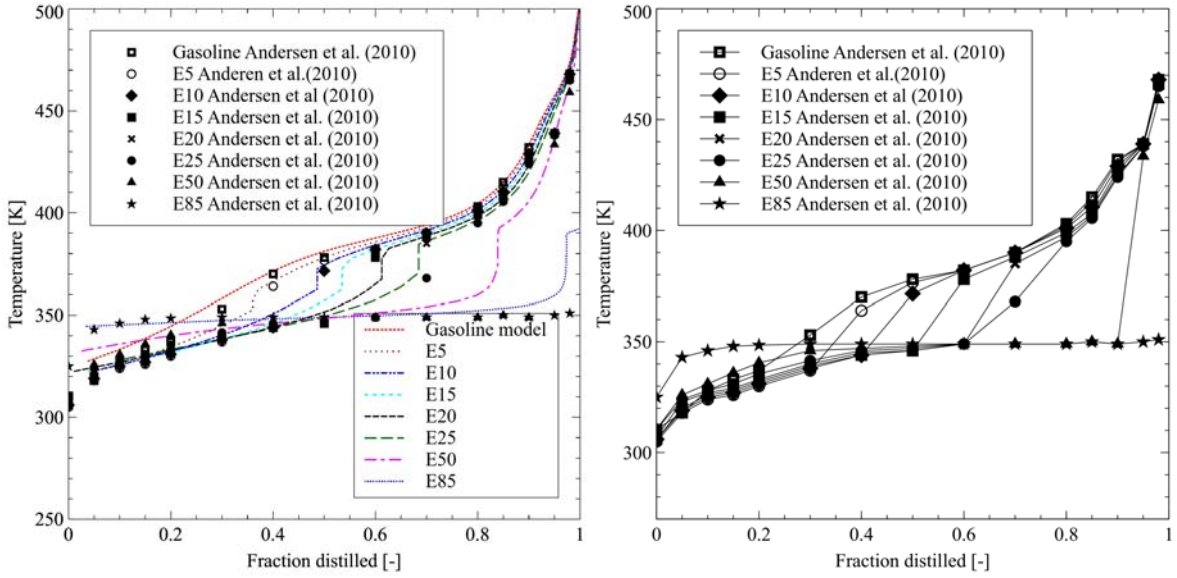

Figure 10: distillation curves for certification and oxygenated fuel calculated with the Rachford-Rice equation and comparison with the experimental values of Ref.[29].

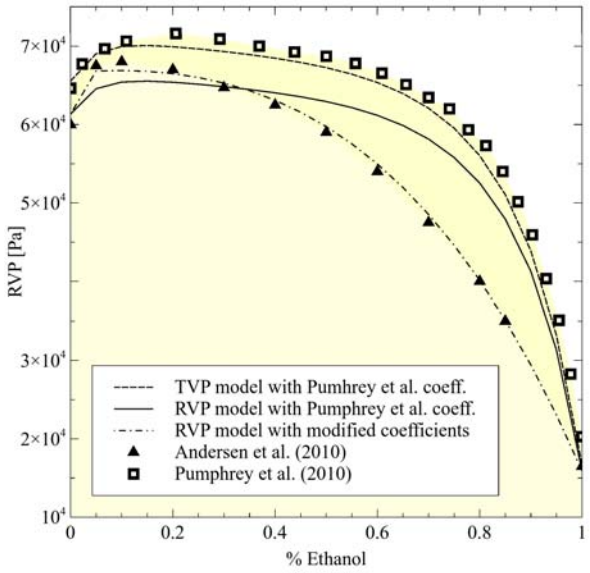

Figure 11: calculation of the TVP and RVP and comparison with data reported by Ref.[17] and Ref.[28]

Andersen et al. obtained a value of RVP for unblended gasoline lower that the one presented by Ref.[17]. Andersen sustained that the data for vapour pressure provided by Ref.[17] was higher than the average data published in literature, and that these differences, of the order of 2-7 kPa, were likely due to the contribution of dissolved air in the data reported by Pumphrey et al. The surrogate of indolene synthesized in this work, was shaped with an RVP similar to the one reported by Andersen, and shows a TVP close to the values presented by Pumphrey et al. The third curve (dash-dotted) plotted in figure 11 shows that it was possible to adjust the coefficients in order to match closely the values reported by Ref.[28]. However, since a rigorous optimization of these coefficients was not made and fell beyond the target of the present work, the values given by Ref.[17] were used for the calculations.
The surrogate shown were used to extract the main thermodynamic and transport characteristics. The properties were calculated with the thermophysical model reported in this work and they were fitted into 5th order polynomial functions of temperature, using a least-squares method; these coefficients were provided with their relative suggested temperature ranges. The coefficients were given for saturation properties and for supercritical properties.

4 Polynomial fittings and accuracy of results

The fitting functions are of the kind of the following polynomial:

$$f(T) = a_5 T^5 + a_4 T^4 + a_3 T^3 + a_2 T^2 + a_1 T + a_0 \qquad (67)$$

f(T) is the generic property and T is the absolute temperature in K. The polynomial fitting was obtained by the regression of 260 (averaged) sampled points from the raw numerical data of each single property.

For the properties enthalpy and entropy, the normal boiling point convention for reference states was adopted, therefore the enthalpy or entropy of a liquid at its boiling point will be considered equal to zero. For these two properties, the polynomial function can be represented as

$$f(T) = a_5\left(T - T_{ref}\right)^5 + a_4\left(T - T_{ref}\right)^4 + a_3\left(T - T_{ref}\right)^3 + a_2\left(T - T_{ref}\right)^2 + a_1\left(T - T_{ref}\right) + a_0 \qquad (68)$$

It is worth underlining that T_{ref} changes with the blend's composition; normal boiling points of the single species employed and the blends are shown in table 5.

An effort was made to fit each property with a single polynomial function. Some of the properties show a dramatic change in slope at about $0.9xT_c$, and the trade off was between accuracy in the near critical or far critical region. We preferred to privilege the data fitting far from the critical point, as they represent more than 95% of the calculated points. Figure 12 shows the case of density, where splines are compared to single polynomial predictive function; the picture illustrates that the use of a spline would give negligible benefits for fitting the liquid phase. The fitting process is illustrated in figures 12 – 20 for the case of indolene. For the sake of compactness, the illustration of the fitting process for the other 7 blends was omitted as it wouldn't have added any substantial information to the work.

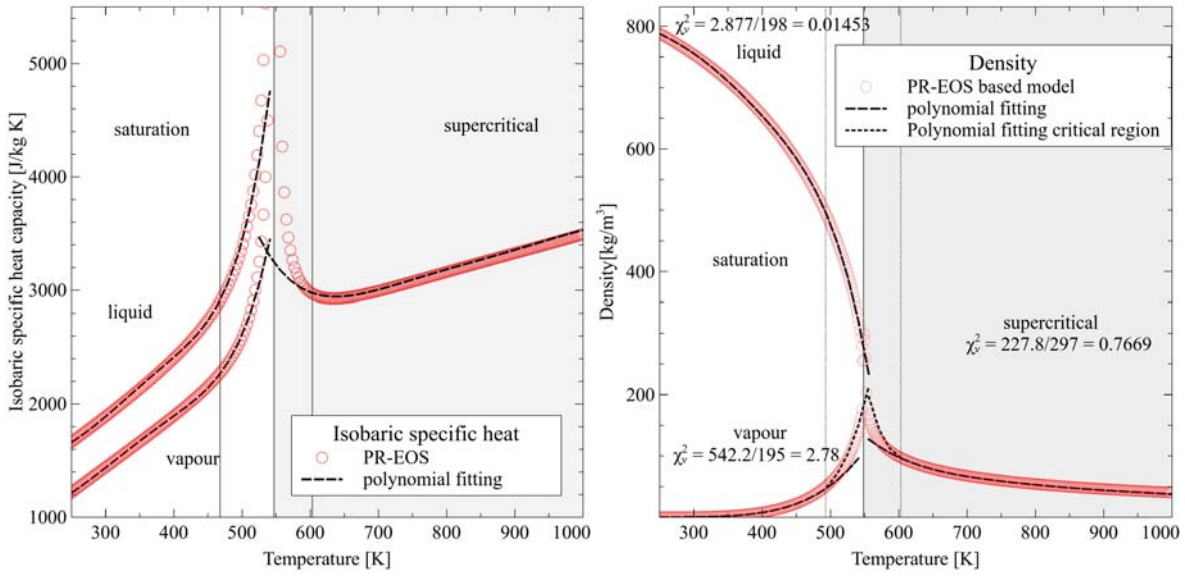

Figure 12: Calculation of the subcritical and supercritical density (left) and isobaric specific heat capacity (right) and 5th order polynomial fitting for indolene.

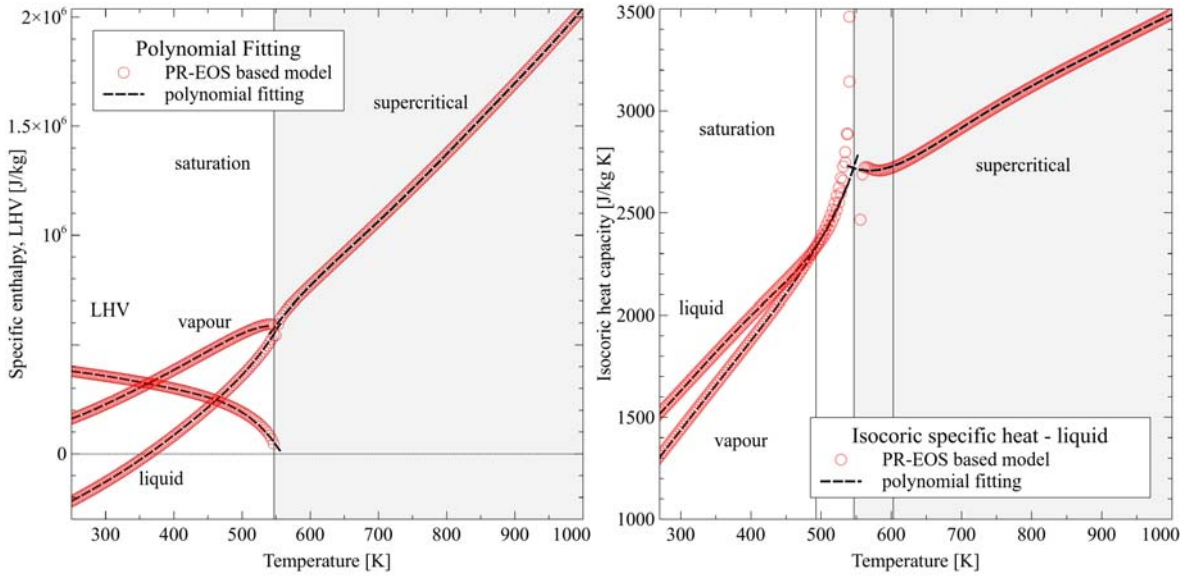

Figure 13: Calculation of subcritical and supercritical isochoric specific heat capacity (left), enthalpy and latent heat of vaporization (right) and 5th order polynomial fitting for indolene.

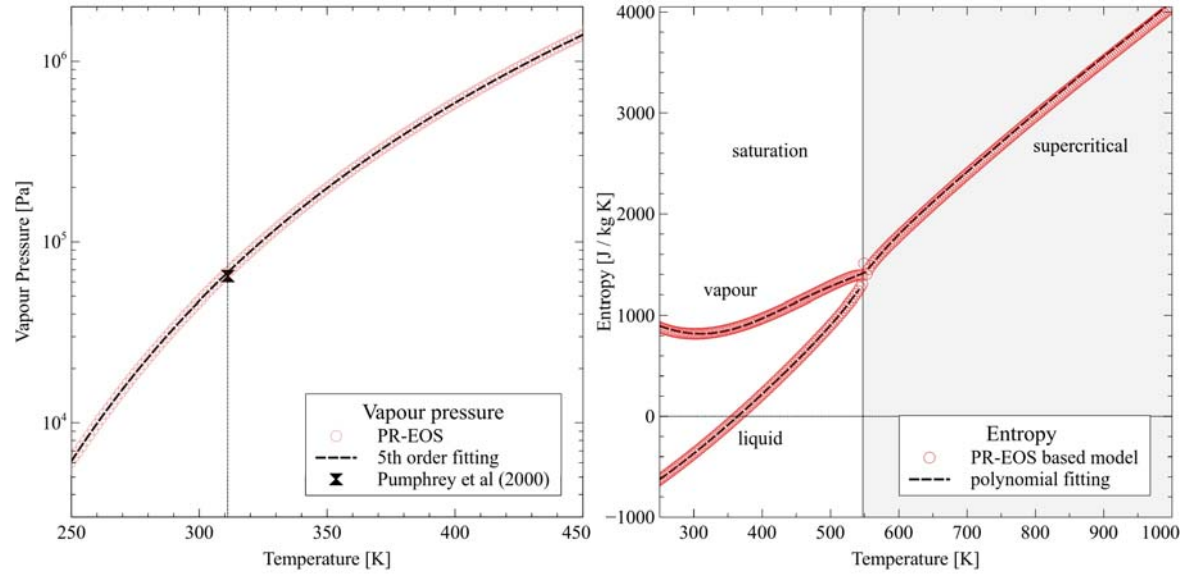

Figure 14: Calculation of subcritical and supercritical entropy (left), vapour pressure (right) and 5th order polynomial fitting for indolene.

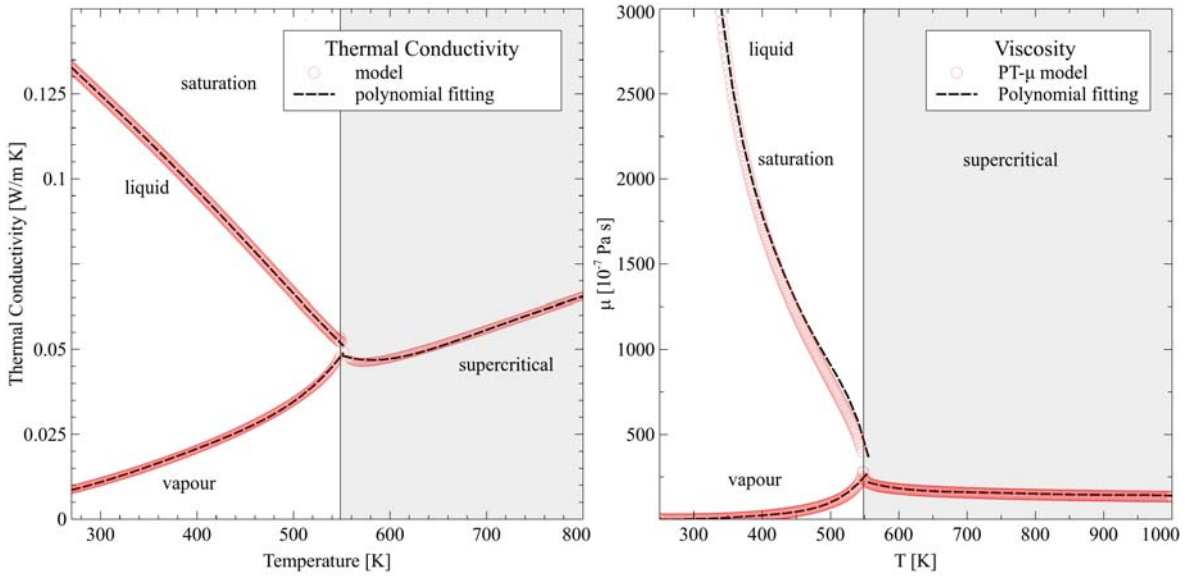

Figure 15: Calculation of subcritical and supercritical viscosity (left), thermal conductivity (right), and 5th order polynomial fitting for indolene.

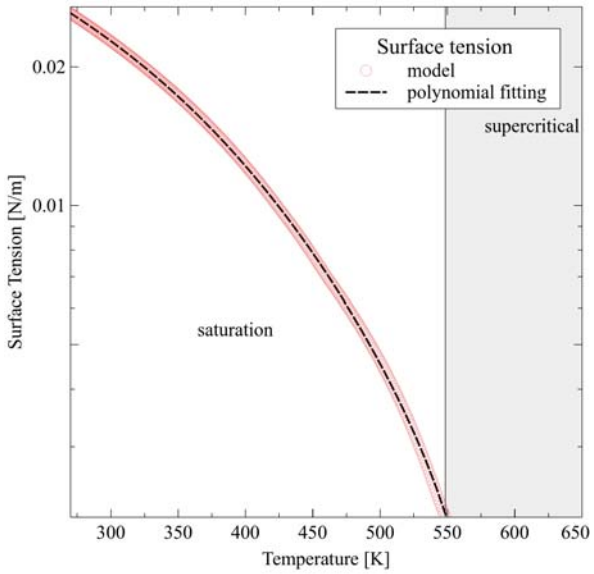

Figure 16: Calculation of surface tension and 5th order polynomial fitting for indolene.

Thermophysical properties of complex mixture are seldom available in literature, and we could not find substantial data for comparing indolene-ethanol mixtures; however, we were able to find good P,V,T reference data for near critical pure ethanol in the work of Bazaev et al. [36], Dillon and Penoncello [37], Skaates and Kay [38], Mousa [39], Chickos and Acree Jr. [40] and some reference data for the density of liquid indolene from Liu et al. [41] to which compare our results.

Being aware that more complicated predictive tools may give more accurate predictions for specific fluids and ranges of applications, the following comparisons are intended to show the potentials and limitations of the correlations proposed. For the comparison we obtained average absolute deviations (AAD) for saturation and near critical vapour pressure, enthalpy of vaporization, liquid and vapour densities, enthalpies, entropies, and specific heat capacities for ethanol, and saturation liquid density for indolene. Bazeav et al. [36] reported values of vapour pressure and density of ethanol for temperature above 373 K. Saturated liquid and vapour densities for ethanol were also reported by Refs. [37][38][39], and saturated liquid and vapour enthalpies and entropies were also found in Ref.[40].

5^{th} order polynomial fitting - deviations ethanol [(a)] and indolene [(b)]			
	N. of data points	AAD %	Ref.
Enthalpy of Vaporization [(a)]	36	3.04	[40]
Sat. Vap. and liq. Enthalpy [(a)]	4	0.13	[37]
Sat. Vap. and liq. Entropy [(a)]	4	1.30	[37]
Sat. Vap. and Liq. Cp [(a)]	4	9.58	[37]
Sat. Vap. and Liq. Cv [(a)]	4	7.90	[37]
Vapour Pressure [(a)]	11	0.39	[36]
	10	7.65	[39]
	6	0.81	[38]
	11	0.61	[37]
Sat. Vapour Density [(a)]	9	6.18	[36]
	8	20.4	[39]
	6	21.3	[38]
	9	6.87	[37]
Sat. Liquid Density [(a)]	9	12.47	[36]
	8	23.87	[39]
	6	12.20	[38]
	9	12.49	[37]
Sat. Liquid Density [(b)]	7	2.20	[41]

Table 6: Comparison of calculations of saturation properties for ethanol and indolene with selected data from literature.

Results from Refs.[36][38][39] are from measurements, while results from Ref.[37] are from calculations. Table 6 shows excellent agreement of predicted values of vapour pressure for ethanol with

respect to selected results from literature. In particular, AAD of 0.39 % was calculated with the data of Bazaev et al. [36]. The worst result for vapour pressure, 7.65 %, was obtained against the data of Mousa [39]; however, Bazaev et al. [36] sustained that measurements obtained by Ref.[39] were not reliable. Excellent agreement was also found for saturated vapour and liquid enthalpies (AAD 0.13%) and entropies (AAD 1.30%) against values extracted from the fundamental equation of state for ethanol proposed by Dillon and Penoncello [37].

Table 6 also shows comparison of calculated saturated vapour and liquid densities versus data reported by Refs.[36][37][38][39], enthalpy of vaporization with Refs.[40], saturated liquid and vapour enthalpies and entropies for ethanol with Ref.[37] and saturated liquid density for indolene with ref.[41]. Not surprisingly, predictions of vapour densities show better agreements than predictions of liquid densities, for ethanol. Best results were obtained with respect to the data of Bazaev et al. [36] and Dillon and Penoncello [37] for the vapour density (AAD respectively 6.18 % and 6.87 %), and against the data of Skaates and Kay [38] for the liquid density (AAD 12.2 %). Figure 17 shows the low errors associated with the predictions over most temperature range and an increase in the error of the vapour and liquid densities, approaching the critical point; this is due to the polynomial fitting and not to the equation of state employed, which would predict better results.

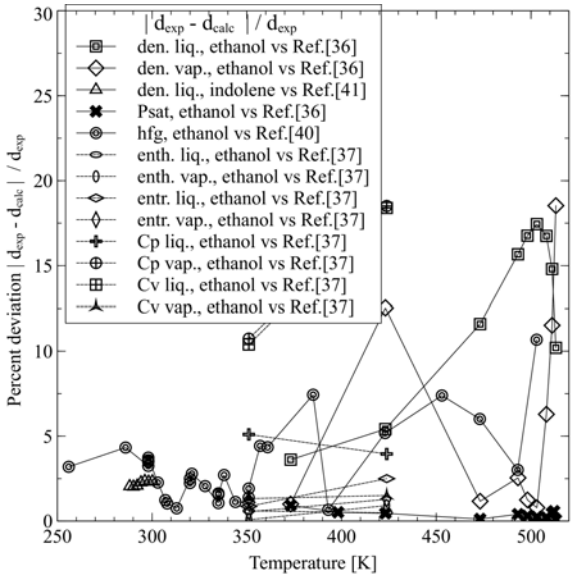

Figure 17: Percent absolute deviation of calculations of saturated properties of ethanol and indolene with selected results from literature.

This is evident from figure 18, where the comparison of vapour densities demonstrates a good

behaviour of the PR-EOS around the critical point and the limitations of the polynomial fitting.

Figure 19 shows a comparison of predicted values from PR-EOS and the polynomial function of enthalpy of vaporization for ethanol against experimental data collected by Chickos and Acree [40]. Their work reported measurement data obtained by several authors and different methods; two singular data points reported were far apart from all the other measurements and no peculiar explanation was given; we decided to exclude these points from our calculation of the errors of figure 17. Figure 19 also suggests that the deviation between the fitted function and the PR-EOS is, in this case, smaller than the variance of scattered measurements over most of the temperature range, but the two become comparable near the critical point.

Figure 20 shows the very good agreement for the vapour pressure over the whole temperature range and, on the right, the tendency of the PR-EOS to underestimate the liquid density. Both behaviours are reflected by the polynomial function.

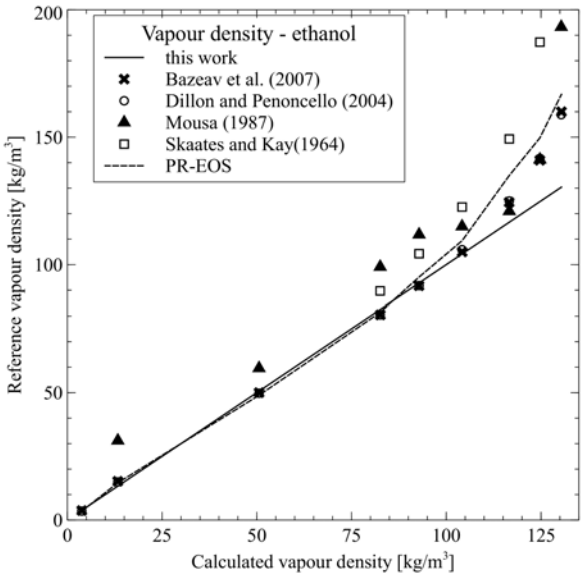

Figure 18: Comparison of calculated and reference data of saturation vapour density for ethanol.

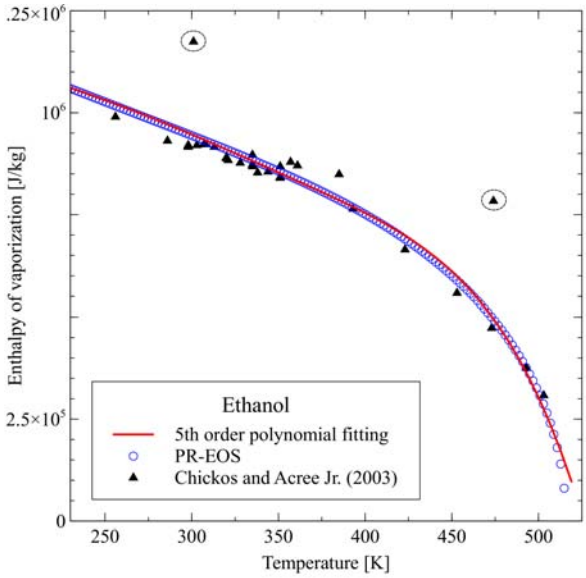

Figure 19: Enthalpy of vaporization for ethanol predicted by PR-EOS and the polynomial relation compared to experimental data from Ref.[40]. Data points in circles were excluded from our calculation of errors.

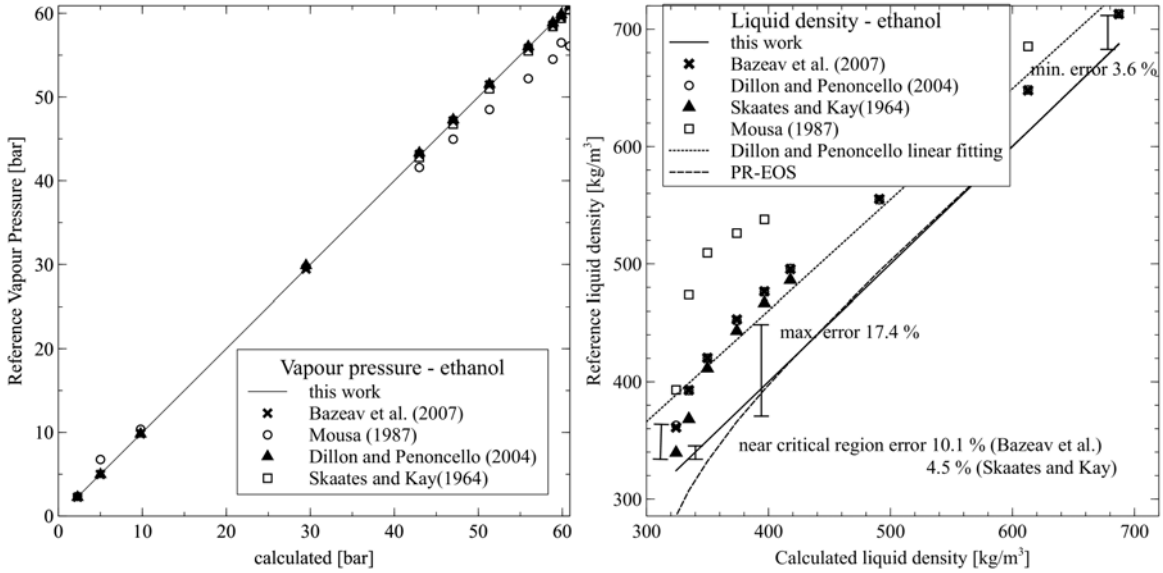

Figure 20: Comparison of calculated and reference data of vapour pressure and density of liquid phase for ethanol.

4.1 Application to Modern Internal Combustion Engines

Cubic EOS are normally not implemented in open source CFD codes and sometimes they are present in commercial codes, but not as a default thermodynamic solver; historically, their use has been restricted to specialized VLE calculations. The use of multi-component real like fuels brought the interest for

cubic EOS among the internal combustion engine community; Kawano et al. [42] implemented a PR-EOS in KIVA 3v to simulate liquid-vapour equilibrium in numerical simulation of flash boiling sprays of multi-component fuels; Neroorkar and Schmidt [43] implemented a PR-EOS in Open FOAM to calculate saturated liquid densities of gasoline-ethanol blends in direct injection engines, Negro and Bianchi [4] used a VTPR-EOS in a homogeneous one-dimensional model for predicting nozzle chocking in superheated liquid fuel injectors, the recent works of Qiu and Reitz [44] [10] report of an implementation of a PR-EOS in KIVA 3v to account for real gas effects and phase change in supercritical injections and fuel condensation, Ma et al. [45] adopted a PR-EOS to account for the consistent thermodynamics in supercritical and transcritical regimes, simulating transcritical n-dodecane injections in a Diesel engine. This brief literature review is certainly not comprehensive, but it gives an idea of the growing interest towards the PR-EOS in engine simulations.

The development of rapid and fairly accurate procedures for the calculation of saturation domain, critical and supercritical regions, is of value for CFD calculation of mixture formation and combustion processes, since most standard CFD packages do not include sophisticated libraries of thermophysical properties. However, whereas a cubic equation of state such as the Peng-Robinson or Soave-Redlick-Kwong is implemented, the procedures generally require a considerable increase in computational effort and, sometimes, instabilities due to the analytical solution. One motivation of the present work is to permit an alternative way to evaluate the saturation, critical, and supercritical region, which substantially reduces the amount of computation required, making the applications of real-like fuels possible with any CFD tool, with a contained loss in accuracy due to the interpolation. We advise two different ways of application of our thermophysical functions: the first way is a direct use for preliminary thermodynamic analysis; the second way consists in the implementation of the thermodynamic functions into CFD codes for the solution of complex flows.

4.1.1 Case Study - Preliminary Assessments of the Potential for Flash Boiling in Subcritical Injections

As an example of direct use of the libraries, we illustrate a preliminary assessments of the potential for flash boiling during a subcritical fuel injection process.

A great challenge in designing gasoline direct injection (GDI) engines is to predict the behaviour of a fuel during the injection process, at different chamber conditions. In modern engines the fuel is sometimes unintentionally superheated before injection and this can significantly alter the spray pattern and, consequently, the air-fuel mixing and, furthermore, generate the risk of vapour lock within the fuel

line [43]. On the other hand, superheated flashing flows have the potential to generate sprays with smaller droplets and more uniform size distributions, thus a better atomization which could, theoretically, improve the mixture formation before combustion [46]. However, the design of a combustion chamber in such an engine may need to take into account these effects of fuel pre-heating, given that this will strongly affect the combustion process. A direct thermodynamic analysis could help assessing the potential for flash boiling sprays; in direct injection engines, flash-boiling occurs at conditions where the chamber pressure is below the saturation pressure of the fuel. Figure 21 shows the loci of typical pressure points at injector inlet and at nozzle exit extracted from W. Zeng et al. [47], and their correlation, on a p-T diagram, with the saturation pressures of different fuels, calculated with the present work. It is immediate to see that the potential for flash-boiling sprays, in typical fuel injection conditions for direct-injection engines, increases for idle and partial-load operations, higher temperatures, and lower contents of ethanol in the blend.

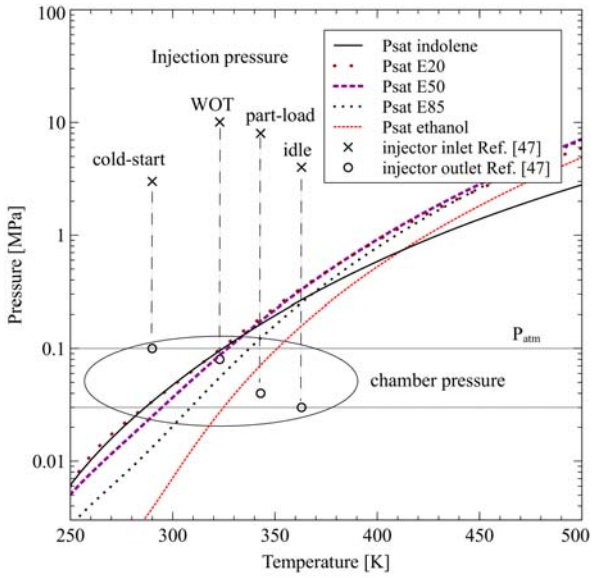

Figure 21: Potential for flash-boiling sprays in typical fuel injection conditions for direct-injection engines: cold-start, idle, part-load, and wide-open-throttle (WOT) operations.

Figure 22 shows the bubble points of different indolene-ethanol mixtures, at different temperatures, calculated with the coefficients presented in this work with respect to the loci of typical chamber pressures for a GDI engine, which is represented by a shaded area in the figure. Further steps of the analysis may include the calculation of non-dimensional quantities that can be useful in estimating the vaporization and condensation regimes and that can guide in the selection of an appropriate phase-change model, when simulating a fuel injection process.

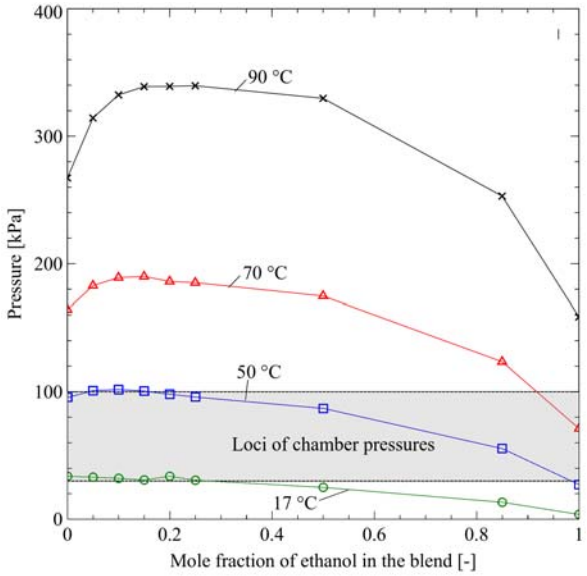

Figure 22: Calculated variation in vapour pressure due to temperature and non-ideal blending, with respect of the loci of typical chamber pressures for a GDI engine, which is represented by a shaded area.

4.1.2 Future works

Our imminent efforts will focus on an implementation of the presented fuel libraries in a fully compressible Eulerian numerical framework with the adoption of a large eddy simulation (LES) method, in order to simulate subcritical and transcritical fuel injection processes and mixture formation. Great emphasis will be given to the accuracy of the predictions and on the assessment of the computational costs required by the numerical libraries, in particular by comparing the results with an analytically solved, PR-EOS based thermodynamic sub-model. Once again, it is important to underline that the properties presented in this work are related to the fuel only. In engine simulations, when the fuel is mixed with air, the resulting mixture will contain nitrogen. In transcritical air-fuel blends, the works of Refs. [31] [32] provide a good reference for the calculation of the critical point of the nitrogen containing blend.

Another intent of application will be the simulation of soot emissions and fuel auto-ignition (in both Spark Ignited and Compression Ignited engines), for which the fuel library here presented is going to be applied as a standard in defining the surrogate of commercial fuels. A detailed chemistry based auto-ignition time look-up table will be coupled with an accurate multi-component fuel injection simulation approach, based on the thermo-physical library presented. This study will focus on reducing the simulation errors and assessing the robustness of the method, and its suitability for simulating

advanced, high efficiency, engine cycles, such as Gasoline Direct Injection Compression Ignition (GDCI), Jet Controlled Compression Ignition (JCCI), Turbulent Jet Ignition (TJI for lean burning), and supercrtitical fuel injection engines.

Table of coefficients: a table containing the 1296 coefficients is included in Appendix A.

Conclusions

Thermodynamic and transport properties of automotive certification fuel surrogate, indolene, and its blends with ethanol E5, E10, E15, E20, E25, E50 and E85, were given in the form of least squares polynomial coefficients, for a subcritical and supercritical range of temperature, up to 1000 K. This format was meant to facilitate predictions and implementation in CFD numerical codes for engine simulations. Properties include enthalpy, latent heat of vaporization, isobaric and isochoric specific heat capacity, entropy, surface tension, thermal conductivity, density, vapour pressure and viscosity.
The theoretical and numerical calculations were carried out at the best of our knowledge and the procedures were validated versus technical data present in literature.

Acknowledgements

This research has been funded by the Italian Government (M.I.U.R) within the project PRIN 2010-11 entitled ”Intensificazione di Processi Catalitici per Energia Pulita, Trasporti a Basse Emissioni e Chimica Sostenibile usando Schiume a Celle Aperte quali Nuovi Materiali Strutturati Avanzati (FOAMS)”. The first author wishes to thank Professor James S. Wallace from the Engine Research and Development Laboratory at the University of Toronto for his technical advice.

Nomenclature

a	substance parameter in PR-EOS	c_1,_,c_4	numerical coefficients in the TVP equation
a_1,_,a_5	coefficients in the polynomial fitting function	Cp	isobaric specific heat capacity
A	parameter in PR-EOS	Cv	isochoric specific heat capacity
ASTM	American Society for Testing and Materials	e_0,_,e_6	parameters in PT-μ model
b	substance parameter in PR-EOS	E	parameter in TVP equation
B	parameter in PR-EOS	E0,_,E85	certification fuel/ethanol blends
c, c_0	corrective terms in PT-μ model	F	parameter in TVP equation

f	fugacity
g^E	Gibbs free energy
h	enthalpy
HCCI	Homogeneous Charge Compression Ignition
k	binary interaction parameter, in PR-EOS
M_W	molecular weight
N	number of components
NIST	National Institute of Standards and Technology
P	pressure
PCCI	premixed charge compression ignition
R	gas constant
R'	parameter in PT-μ model
RVP	Reid vapour pressure
s	entropy
S	liquid stock in RVP equations
SIDI	spark-ignition direct injection
T	temperature
T'	pseudo temperature in PT-μ equation
Td	temperature correction in PT-μ model
T_3	triple point temperature
TSI	transonic combustion
TVP	true vapour pressure
v	specific volume
Z	compressibility

Greek letters

β	parameter in PT-μ model
φ	fugacity coefficient
γ	activity coefficient
Λ	parameter in Wilson equation
λ	thermal conductivity
ω	acentric factor
μ	viscosity
ρ	density
σ	surface tension

Subscripts

bo	boiling
C	critical
i, j, k	component -i, -j, -k
l	liquid
LA	liquid average
gas	gas
m	mixture
min	minimum
max	maximum
r	reduced
ref	reference state
sat	saturation
v	vapour

References

[1] Pons L, Darabiha N, Candel S, Ribert G, Yang V. Mass transfer and combustion in transcritical non-premixed counterflows. Combust Theory Model 2009;13:57–81. doi:10.1080/13647830802368821.

[2] Boer C De, Chang J, Shetty S. Transonic Combustion - A Novel Injection-Ignition System for Improved Gasoline Engine Efficiency. Sae Pap 2010-01-2110 2010.

[3] Qiu L, Reitz RD. Simulation of supercritical fuel injection with condensation. Int J Heat Mass Transf 2014;79:1070–86. doi:10.1016/j.ijheatmasstransfer.2014.08.081.

[4] Negro S, Bianchi GM. Superheated fuel injection modeling: An engineering approach. Int J Therm Sci 2011;50:1460–71. doi:10.1016/j.ijthermalsci.2011.03.028.

[5] Mc Bride J, Gordon S, Reno A. Coefficients for Calculating Thermodynamic and Transport Properties of Individual Species. NASA Tech Memo 4513 1993;4513:98.

[6] Svehla RA. Transport coefficients for the NASA Lewis Chemical Equilibrium Program. NASA Tech Memo 4647 1995:29.

[7] Peng D-Y, Robinson DB. A New Two-Constant Equation of State. Ind Eng Chem Fundam 1976;15:59–64. doi:10.1021/i160057a011.

[8] Rachford HH Jr and Rice JD. Procedure for Use of Electronic Digital Computers in Calculating Flash Vaporization Hydrocarbon Equilibrium. J Pet Technol 1952;4:327–8. doi:10.2118/952327-G.

[9] Wilson GM. A Modified Redlich-Kwong Equation of State, Application to General Physical Data Calculations. 65 th Natl. AIChE Meet., Paper 15-C, Cleveland, Ohio, USA: 4–7 May; 1969.

[10] Sastri SRS. and Rao KK. A simple method to predict surface tension of organic liquids. Chem Eng J 1994:181–6.

[11] Curl RF and Pitzer KS. The Volumetric and Thermodynamic Properties of Fluids. III. Empirical Equation for the Second Virial Coefficient. J Phys Chem 1956;470:7–8. doi:-10.1021/ja01567a007.

[12] Chemical Engineering Research Information Center (CHERIC). Korean Thermophysical Properties Data Bank 2013. http://www.cheric.org/research/kdb/.

[13] Latini G, Pacetti M. The Thermal Conductivity of Liquids - A Critical Survey. 15th Int. Therm. Conduct. Conf., 1977, p. 245–53. doi:10.1007/978-1-4615-9083-5_31.

[14] Fan TB, Wang LS. A viscosity model based on Peng-Robinson equation of state for light hydrocarbon liquids and gases. Fluid Phase Equilib 2006;247:59–69. doi:10.1016/j.fluid.2006.06.008.

[15] Onken U, Rarey-Nies J, Gmehling JG. The Dortmund Data Bank: A computerized system for retrieval, correlation, and prediction of thermodynamic properties of mixtures. Int J Thermophys 1989;10:739–47. doi:10.1007/BF00507993.

[16] Solórzano-Zavala M, Barragán-Aroche F, Bazúa E. Comparative study of mixing rules for cubic equations of state in the prediction of multicomponent vapor-liquid equilibria. Fluid Phase Equilib 1996;122:99–116. doi:10.1016/0378-3812(96)03028-2.

[17] Pumphrey JA, Brand JI, Scheller WA. Vapour pressure measurements and predictions for alcohol – gasoline blends. Fuel 2000;79:1405–11.

[18] Friend DG, Huber ML. Thermophysical property standard reference data from NIST. Int J Thermophys 1994;15:1279–88. doi:10.1007/BF01458836.

[19] J. Gmehling, U. Onken, W. Arlt, P. Grenzheuser, U. Weidlich, B. Kolbe JR. Chemistry Data Series, Volume I, Vapor-Liquid Equilibrium Data Collection. Frankfurt: 1989.

[20] Hull A, Kronberg B, van Stam J, Golubkov I, Kristensson J. Vapor−Liquid Equilibrium of Binary Mixtures. 1. Ethanol + 1-Butanol, Ethanol + Octane, 1-Butanol + Octane. J Chem Eng Data 2006;51:1996–2001. doi:10.1021/je0600045.

[21] EPA Environmental Protection Agency, Office of Air Quality, Emission Factor IG. Emission Factor Documentation for AP-42 Organic Liquid Storage Tanks Final Report. 2006.

[22] Campbell JM. Gas Conditioning and Processing. Gas Cond. Process., Norman, OK, USA.: Campbell Petroleum Series; 1984.

[23] Straub J and Nitsche K. Isochoric heat capacity Cv at the critical point of SF 6 under micro- and earth-gravity: Results of the german spacelab mission D1. Fluid Phase Equilib 1993;88:183–208.

[24] Moran MJ, Shapiro HN, Boettner DD, Bailey M. Fundamentals Of Engineering Thermodynamics. 7th ed. Wiley; 2010. doi:10.1177/004057368303900411.

[25] P. Phillips. The viscosity of carbondioxide. Proc R Soc 1912;87A:48.

[26] Guo X-Q, Wang L-S, Rong S-X, Guo T-M. Viscosity model based on equations of state for hydrocarbon liquids and gases. Fluid Phase Equilib 1997;139:405–21. doi:10.1016/S0378-3812(97)00156-8.

[27] ASTM D86-15 Developed by Subcommittee: D02.08. Standard Test Method for Distillation of Petroleum Products and Liquid Fuels at Atmospheric Pressure. B Stand 2015;05.01:1–27. doi:10.1520/D0086-15.

[28] Andersen VF, Anderson JE, Wallington TJ, Mueller S a., Nielsen OJ. Vapor pressures of alcohol-gasoline blends. Energy and Fuels 2010;24:3647–54. doi:10.1021/ef100254w.

[29] Andersen VF, Anderson JE, Wallington TJ, Mueller S a., Nielsen OJ. Distillation curves for alcohol-gasoline blends. Energy and Fuels 2010;24:2683–91. doi:10.1021/ef9014795.

[30] Greenfield ML. Development of Model Fuels With Volatilities That Resemble Those of Real Fuels. Fuel Chem Div Prepr 2002;47:209–10.

[31] Heidemann RA, Khalil AM. The calculation of critical points. AIChE J 1980;26:769–79. doi:10.1002/aic.690260510.

[32] Peng D, Robinson DB. A rigorous method for predicting the critical properties of

multicomponent systems from an equation of state. AIChE J 1977;23:137–44. doi:10.1002/aic.690230202.

[33] Cai J, Hu Y, Prausnitz JM. Simplified critical-point criteria for some multicomponent systems. Chem Eng Sci 2010;65:2443–53. doi:10.1016/j.ces.2009.11.024.

[34] Cotterman RL, Bender R, Prausnitz JM. Phase equilibria for mixtures containing very many components. Development and application of continuous thermodynamics for chemical process design. Ind Eng Chem Process Des Dev 1985;24:194–203. doi:10.1021/i200028a033.

[35] Valderrama JO. The State of the Cubic Equations of State. Ind Eng Chem Res 2003;42:1603–18. doi:10.1021/ie020447b.

[36] Bazaev AR, Abdulagatov IM, Bazaev EA, Abdurashidova A. PVT Measurements for Pure Ethanol in the Near-Critical and Supercritical Regions 2007;28:1–3. doi:10.1007/s10765-007-0158-2.

[37] Dillon HE, Penoncello SG. A Fundamental Equation for Calculation of the Thermodynamic Properties of Ethanol. Int J Thermophys 2004;25:321–35.

[38] J. M. Skaates and W. B. Kay. The phase relations of binary systems that form azeotropes. Chem Eng Sci 1964;19:431–44.

[39] A. H. N. Mousa. Heat of Vaporization and Vapour Pressure of Ethanol from 20 kPa to the Critical Point. J Chem Eng Jap 1987:635–7.

[40] Chickos JS, Jr WEA. Enthalpies of Vaporization of Organic and Organometallic Compounds , 1880 – 2002 Enthalpies of Vaporization of Organic and Organometallic Compounds , 2016;519:1880–2002. doi:10.1063/1.1529214.

[41] Liu YC, Savas AJ, Avedisian CT. Comparison of the Burning Characteristics of Indolene and Commercial Grade Gasoline Droplets without Convection 2012.

[42] Kawano D, Ishii H, Suzuki H, Goto Y, Odaka M, Senda J. Numerical study on flash-boiling spray of multicomponent fuel. Heat Transf Res 2006;35:369–85. doi:10.1002/htj.20117.

[43] Neroorkar K, Schmidt D. Modeling of vapor-liquid equilibrium of gasoline-ethanol blended fuels for flash boiling simulations. Fuel 2011;90:665–73. doi:10.1016/j.fuel.2010.09.035.

[44] Qiu L, Reitz RD. Condensation processes in a motoring engine. J Supercrit Fluids 2014;90:84–100. doi:http://dx.doi.org/10.1016/j.supflu.2014.03.013.

[45] Ma PC, Bravo L. Supercritical and transcritical real-fluid mixing in diesel engine applications, Stanford University: Proceedings of the CTR Summer Program; 2014, p. 99–108.

[46] Negro S, Brusiani F, Bianchi GM. A Numerical Model for Flash Boiling of Gasoline-Ethanol Blends in Fuel Injector Nozzles. SAE Int J Fuels Lubr 2011;4:237–56. doi:10.4271/2011-24-0003.

[47] Zeng W, Xu M, Zhang M, Zhang Y, Cleary DJ. Macroscopic characteristics for direct-injection multi-hole sprays using dimensionless analysis. Exp Therm Fluid Sci 2012;40:81–92. doi:10.1016/j.expthermflusci.2012.02.003.

Appendix A

Indolene

Property	a_5	a_4	a_3	a_2	a_1	a_0	validity range
Enthalpy liquid	3.9241E-07	-7.1809E-04	5.2098E-01	-1.8455E+02	3.3581E+04	-2.7966E+06	[260 K, Tc]
Enthalpy vapour	-4.5077E-07	8.2546E-04	-6.0109E-01	2.1863E+02	-3.8315E+04	2.6836E+06	[260 K, Tc]
Enthalpy supercritical	1.1187E-07	-4.4935E-04	7.1687E-01	-5.6684E+02	2.2492E+05	-3.5428E+07	[Tc, 1000 K]
Latent heat vaporization	-3.2798E-07	5.3352E-04	-3.4210E-01	1.0709E+02	-1.6727E+04	1.4492E+06	[260 K, Tc]
Cp liquid	3.7062E-09	-5.7755E-06	3.5182E-03	-1.0408E+00	1.5331E+02	-7.6473E+03	[260 K, Tc]
Cp vapour	2.3684E-09	-3.7108E-06	2.2733E-03	-6.7875E-01	1.0299E+02	-5.4487E+03	[260 K, Tc]
Cp supercritical	-3.2707E-10	1.3786E-06	-2.3145E-03	1.9346E+00	-8.0331E+02	1.3521E+05	[Tc, 1000 K]
Cv liquid	8.3352E-10	-1.3265E-06	8.1416E-04	-2.4004E-01	3.7506E+01	-1.2821E+03	[260 K, Tc]
Cv vapour	2.2565E-10	-3.2312E-07	1.8125E-04	-5.0014E-02	1.1247E+01	-2.6056E+02	[260 K, Tc]
Cv supercritical	-1.6819E-10	6.9708E-07	-1.1476E-03	9.3706E-01	-3.7720E+02	6.2323E+04	[Tc, 1000 K]
Entropy liquid	2.9097E-10	-4.8871E-07	3.1922E-04	-9.6442E-02	1.8087E+01	-2.4825E+03	[260 K, Tc]
Entropy vapour	8.4266E-10	-1.6683E-06	1.2488E-03	-4.2835E-01	6.5422E+01	-2.5071E+03	[260 K, Tc]
Entropy supercritical	2.0390E-10	-8.1321E-07	1.2897E-03	-1.0178E+00	4.0588E+02	-6.4363E+04	[Tc, 1000 K]
Surface tension	-4.8520E-15	8.9314E-12	-6.1211E-09	2.0316E-06	-4.4721E-04	7.8798E-02	[260 K, Tc]
Thermal cond. liquid	2.6422E-15	-2.6940E-12	3.1162E-10	3.8035E-07	-3.9718E-04	2.1664E-01	[260 K, Tc]
Thermal cond. vapour	2.3846E-14	-3.8713E-11	2.4484E-08	-7.3670E-06	1.1085E-03	-6.4033E-02	[260 K, Tc]
Thermal cond. supercr.	-1.3983E-14	5.6271E-11	-9.0009E-08	7.1536E-05	-2.8152E-02	4.4220E+00	[Tc, 1000 K]
Density liquid	-2.2351E-10	3.5086E-07	-2.1880E-04	6.5739E-02	-9.9974E+00	1.4459E+03	[260 K, Tc]
Density vapour	1.4633e-10	-2.4299E-07	1.6382E-04	-5.5383E-02	9.3268E+00	-6.2367E+02	[260 K, Tc]
Density supecritical	-9.5058E-11	3.8624E-07	-6.2440E-04	5.0223E-01	-2.0119E+02	3.2216E+04	[Tc, 1000 K]
Saturation pressure	-5.5038e-07	1.2401E-03	-8.5099E-01	2.6526E+02	-3.9483E+04	2.2882E+06	[260 K, Tc]
Viscosity liquid	-2.0166E-08	4.5643E-05	-4.1398E-02	1.8835E+01	-4.3129E+03	4.0086E+05	[260 K, Tc]
Viscosity vapour	1.0197E-10	-1.5317E-07	9.2915E-05	-2.7342E-02	3.7876E+00	-1.8904E+02	[260 K, Tc]
Viscosity supercritical	-7.4518E-11	3.0096E-07	-4.8339E-04	3.8611E-01	-1.5352E+02	2.4497E+04	[Tc, 1000 K]

E5

Property	a_5	a_4	a_3	a_2	a_1	a_0	validity range
Enthalpy liquid	3.8455E-07	-7.0805E-04	5.1744E-01	-1.8482E+02	3.3960E+04	-2.8532E+06	[260 K, Tc]
Enthalpy vapour	-3.8497E-07	7.0759E-04	-5.1847E-01	1.9030E+02	-3.3577E+04	2.3856E+06	[260 K, Tc]

Enthalpy supercritical	1.3341E-07	-5.3487E-04	8.5162E-01	-6.7214E+02	2.6573E+05	-4.1690E+07	[Tc, 1000 K]
Latent heat vaporization	-7.6951E-07	1.4156E-03	-1.0359E+00	3.7512E+02	-6.7535E+04	5.2388E+06	[260 K, Tc]
Cp liquid	1.3737E-08	-2.4664E-05	1.7550E-02	-6.1768E+00	1.0788E+03	-7.3273E+04	[260 K, Tc]
Cp vapour	9.3537E-09	-1.6840E-05	1.2012E-02	-4.2383E+00	7.4367E+02	-5.0855E+04	[260 K, Tc]
Cp supercritical	-8.2331E-10	3.3929E-06	-5.5639E-03	4.5381E+00	-1.8393E+03	2.9900E+05	[Tc, 1000 K]
Cv liquid	2.3061E-09	-3.6031E-06	2.1809E-03	-6.3571E-01	9.1411E+01	-3.6994E+03	[260 K, Tc]
Cv vapour	1.6952E-09	-2.5977E-06	1.5573E-03	-4.5435E-01	6.8263E+01	-3.2771E+03	[260 K, Tc]
Cv supercritical	-2.2908E-10	9.3939E-07	-1.5299E-03	1.2363E+00	-4.9365E+02	8.0362E+04	[Tc, 1000 K]
Entropy liquid	6.8717E-10	-1.2726E-06	9.3051E-04	-3.3107E-01	6.2441E+01	-5.7905E+03	[260 K, Tc]
Entropy vapour	-7.7497E-10	1.5001E-06	-1.1863E-03	4.8833E-01	-1.0347E+02	9.7065E+03	[260 K, Tc]
Entropy supercritical	4.6072E-10	-1.8337E-06	2.8986E-03	-2.2756E+00	8.9334E+02	-1.3925E+05	[Tc, 1000 K]
Surface tension	-3.5037E-15	6.5986E-12	-4.5752E-09	1.5359E-06	-3.6820E-04	7.3561E-02	[260 K, Tc]
Thermal cond. liquid	2.5409E-15	-2.4760E-12	1.4037E-10	4.4924E-07	-4.1532E-04	2.1956E-01	[260 K, Tc]
Thermal cond. vapour	2.0845E-14	-3.3398E-11	2.0867E-08	-6.1839E-06	9.2348E-04	-5.2785E-02	[260 K, Tc]
Thermal cond. supercr.	-1.6127E-14	6.4795E-11	-1.0345E-07	8.2047E-05	-3.2224E-02	5.0476E+00	[Tc, 1000 K]
Density liquid	-3.4415E-10	5.5259E-07	-3.4999E-04	1.0707E-01	-1.6291E+01	1.8161E+03	[260 K, Tc]
Density vapour	1.5967E-10	-2.6572E-07	1.7936E-04	-6.0697E-02	1.0232E+01	-6.8503E+02	[260 K, Tc]
Density supecritical	-4.1123E-11	1.7019E-07	-2.8084E-04	2.3120E-01	-9.5144E+01	1.5758E+04	[Tc, 1000 K]
Saturation pressure	7.7916E-07	-3.0838E-04	-1.2545E-01	9.3688E+01	-1.8947E+04	1.2910E+06	[260 K, Tc]
Viscosity liquid	-2.8413E-08	6.3634E-05	-5.6974E-02	2.5521E+01	-5.7356E+03	5.2089E+05	[260 K, Tc]
Viscosity vapour	7.9978E-11	-1.0641E-07	5.4748E-05	-1.2190E-02	8.4677E-01	3.4740E+01	[260 K, Tc]
Viscosity supercritical	-7.3686E-11	2.9738E-07	-4.7728E-04	3.8093E-01	-1.5134E+02	2.4136E+04	[Tc, 1000 K]

E10

Property	a_5	a_4	a_3	a_2	a_1	a_0	validity range
Enthalpy liquid	2.0573E-07	-3.3513E-04	2.1412E-01	-6.4505E+01	1.0707E+04	-1.1037E+06	[260 K, Tc]
Enthalpy vapour	-1.9616E-07	3.1500E-04	-1.9992E-01	6.4162E+01	-9.2004E+03	5.5814E+05	[260 K, Tc]
Enthalpy supercritical	1.2856E-07	-5.1557E-04	8.2111E-01	-6.4823E+02	2.5644E+05	-4.0251E+07	[Tc, 1000 K]
Latent heat vaporization	-4.0189E-07	6.5013E-04	-4.1403E-01	1.2867E+02	-1.9907E+04	1.6619E+06	[260 K, Tc]
Cp liquid	4.7408E-09	-7.3791E-06	4.4900E-03	-1.3274E+00	1.9422E+02	-9.8466E+03	[260 K, Tc]
Cp vapour	2.9888E-09	-4.6700E-06	2.8526E-03	-8.4890E-01	1.2717E+02	-6.7670E+03	[260 K, Tc]
Cp supercritical	-6.5369E-10	2.7075E-06	-4.4636E-03	3.6611E+00	-1.4923E+03	2.4449E+05	[Tc, 1000 K]
Cv liquid	1.5337E-09	-2.4693E-06	1.5393E-03	-4.6294E-01	7.0461E+01	-3.1085E+03	[260 K, Tc]
Cv vapour	1.1279E-09	-1.7814E-06	1.0984E-03	-3.2974E-01	5.2457E+01	-2.5908E+03	[260 K, Tc]
Cv supercritical	-1.9991E-10	8.2498E-07	-1.3524E-03	1.1000E+00	-4.4161E+02	7.2431E+04	[Tc, 1000 K]
Entropy liquid	4.0154E-10	-6.7271E-07	4.4009E-04	-1.3594E-01	2.4746E+01	-2.9708E+03	[260 K, Tc]

Entropy vapour	1.0089E-09	-1.9889E-06	1.4876E-03	-5.1394E-01	7.9928E+01	-3.3394E+03	[260 K, Tc]
Entropy supercritical	-1.0835E-11	4.0186E-08	-5.5797E-05	3.3770E-02	-1.4626E+00	-1.7806E+03	[Tc, 1000 K]
Surface tension	-2.1805E-15	4.2889E-12	-3.0297E-09	1.0348E-06	-2.8739E-04	6.8151E-02	[260 K, Tc]
Thermal cond. liquid	2.5276E-15	-2.3827E-12	3.2664E-11	5.0501E-07	-4.3295E-04	2.2262E-01	[260 K, Tc]
Thermal cond. vapour	2.4271E-14	-3.8906E-11	2.4307E-08	-7.2212E-06	1.0750E-03	-6.1160E-02	[260 K, Tc]
Thermal cond. supercr.	-1.4554E-14	5.8497E-11	-9.3446E-08	7.4161E-05	-2.9141E-02	4.5700E+00	[Tc, 1000 K]
Density liquid	-3.2358E-10	5.1411E-07	-3.2270E-04	9.7811E-02	-1.4789E+01	1.7227E+03	[260 K, Tc]
Density vapour	1.6750E-10	-2.7764E-07	1.8656E-04	-6.2831E-02	1.0540E+01	-7.0218E+02	[260 K, Tc]
Density supecritical	-1.0654E-10	4.3182E-07	-6.9621E-04	5.5833E-01	-2.2292E+02	3.5556E+04	[Tc, 1000 K]
Saturation pressure	1.4148E-06	-1.0531E-03	2.2460E-01	1.0810E+01	-9.0267E+03	8.0944E+05	[260 K, Tc]
Viscosity liquid	-3.0146E-08	6.7150E-05	-5.9802E-02	2.6647E+01	-5.9573E+03	5.3820E+05	[260 K, Tc]
Viscosity vapour	-1.1637E-11	7.4421E-08	-8.5514E-05	4.1369E-02	-9.2295E+00	7.8208E+02	[260 K, Tc]
Viscosity supercritical	-1.0661E-10	4.2802E-07	-6.8287E-04	5.4128E-01	-2.1332E+02	3.3629E+04	[Tc, 1000 K]

E15

Property	a_5	a_4	a_3	a_2	a_1	a_0	validity range
Enthalpy liquid	1.7880E-07	-2.8822E-04	1.8282E-01	-5.4522E+01	9.2141E+03	-1.0238E+06	[260 K, Tc]
Enthalpy vapour	-1.7017E-07	2.6946E-04	-1.6939E-01	5.4333E+01	-7.6793E+03	4.7972E+05	[260 K, Tc]
Enthalpy supercritical	1.3897E-07	-5.5671E-04	8.8560E-01	-6.9834E+02	2.7574E+05	-4.3190E+07	[Tc, 1000 K]
Latent heat vaporization	-3.4897E-07	5.5768E-04	-3.5221E-01	1.0886E+02	-1.6893E+04	1.5036E+06	[260 K, Tc]
Cp liquid	5.4190E-09	-8.4458E-06	5.1475E-03	-1.5252E+00	2.2314E+02	-1.1457E+04	[260 K, Tc]
Cp vapour	3.4105E-09	-5.3354E-06	3.2641E-03	-9.7316E-01	1.4541E+02	-7.8032E+03	[260 K, Tc]
Cp supercritical	-6.4126E-10	2.6575E-06	-4.3836E-03	3.5978E+00	-1.4676E+03	2.4067E+05	[Tc, 1000 K]
Cv liquid	1.8436E-09	-2.9731E-06	1.8584E-03	-5.6100E-01	8.4975E+01	-3.9095E+03	[260 K, Tc]
Cv vapour	1.5688E-09	-2.5017E-06	1.5569E-03	-4.7146E-01	7.3640E+01	-3.8098E+03	[260 K, Tc]
Cv supercritical	-2.1267E-10	8.7613E-07	-1.4338E-03	1.1643E+00	-4.6686E+02	7.6391E+04	[Tc, 1000 K]
Entropy liquid	2.6683E-10	-4.4450E-07	2.9149E-04	-8.9784E-02	1.8062E+01	-2.6296E+03	[260 K, Tc]
Entropy vapour	7.9019E-10	-1.6344E-06	1.2658E-03	-4.4698E-01	7.0053E+01	-2.7120E+03	[260 K, Tc]
Entropy supercritical	3.8550E-10	-1.5334E-06	2.4229E-03	-1.9019E+00	7.4779E+02	-1.1673E+05	[Tc, 1000 K]
Surface tension	-1.1524E-15	2.5054E-12	-1.8497E-09	6.5711E-07	-2.2679E-04	6.4024E-02	[260 K, Tc]
Thermal cond. liquid	2.7360E-15	-2.6989E-12	2.2015E-10	4.5751E-07	-4.3332E-04	2.2461E-01	[260 K, Tc]
Thermal cond. vapour	3.8156E-14	-6.2198E-11	3.9493E-08	-1.2019E-05	1.8089E-03	-1.0441E-01	[260 K, Tc]
Thermal cond. supercr.	-1.5656E-14	6.2836E-11	-1.0022E-07	7.9395E-05	-3.1144E-02	4.8749E+00	[Tc, 1000 K]
Density liquid	-3.0164E-10	4.7508E-07	-2.9635E-04	8.9315E-02	-1.3481E+01	1.6459E+03	[260 K, Tc]
Density vapour	1.6880E-10	-2.7697E-07	1.8416E-04	-6.1358E-02	1.0180E+01	-6.7050E+02	[260 K, Tc]
Density supecritical	-9.5917E-11	3.8928E-07	-6.2856E-04	5.0494E-01	-2.0202E+02	3.2312E+04	[Tc, 1000 K]

Saturation pressure	1.8047E-06	-1.5165E-03	4.4522E-01	-4.2091E+01	-2.6118E+03	4.9386E+05	[260 K, Tc]
Viscosity liquid	-3.2833E-08	7.2409E-05	-6.3860E-02	2.8188E+01	-6.2451E+03	5.5931E+05	[260 K, Tc]
Viscosity vapour	1.6449E-10	-2.6082E-07	1.6781E-04	-5.3448E-02	8.3300E+00	-5.0415E+02	[260 K, Tc]
Viscosity supercritical	-1.0628E-10	4.2630E-07	-6.7947E-04	5.3804E-01	-2.1181E+02	3.3358E+04	[Tc, 1000 K]

E20

Property	a_5	a_4	a_3	a_2	a_1	a_0	validity range
Enthalpy liquid	1.5079E-07	-2.3859E-04	1.4907E-01	-4.3511E+01	7.5212E+03	-9.2971E+05	[260 K, Tc]
Enthalpy vapour	-3.7380E-07	6.0888E-04	-3.8900E-01	1.2307E+02	-1.8060E+04	1.0972E+06	[260 K, Tc]
Enthalpy supercritical	1.2775E-07	-5.1186E-04	8.1443E-01	-6.4236E+02	2.5391E+05	-3.9806E+07	[Tc, 1000 K]
Latent heat vaporization	-5.2460E-07	8.4747E-04	-5.3807E-01	1.6658E+02	-2.5581E+04	2.0269E+06	[260 K, Tc]
Cp liquid	5.9228E-09	-9.1849E-06	5.5671E-03	-1.6395E+00	2.3789E+02	-1.2135E+04	[260 K, Tc]
Cp vapour	3.7334E-09	-5.8153E-06	3.5408E-03	-1.0501E+00	1.5563E+02	-8.3137E+03	[260 K, Tc]
Cp supercritical	-6.2422E-10	2.5885E-06	-4.2726E-03	3.5092E+00	-1.4326E+03	2.3520E+05	[Tc, 1000 K]
Cv liquid	2.0921E-09	-3.3560E-06	2.0858E-03	-6.2563E-01	9.3611E+01	-4.3111E+03	[260 K, Tc]
Cv vapour	1.7322E-09	-2.7508E-06	1.7043E-03	-5.1341E-01	7.9316E+01	-4.0946E+03	[260 K, Tc]
Cv supercritical	-2.0789E-10	8.5688E-07	-1.4031E-03	1.1399E+00	-4.5727E+02	7.4905E+04	[Tc, 1000 K]
Entropy liquid	3.0257E-10	-5.0306E-07	3.2997E-04	-1.0265E-01	2.0377E+01	-2.8195E+03	[260 K, Tc]
Entropy vapour	9.0335E-10	-1.8577E-06	1.4354E-03	-5.0883E-01	8.0720E+01	-3.3487E+03	[260 K, Tc]
Entropy supercritical	-7.1406E-11	2.7965E-07	-4.3108E-04	3.2506E-01	-1.1341E+02	1.5301E+04	[Tc, 1000 K]
Surface tension	-1.8388E-16	8.0540E-13	-7.1167E-10	2.8817E-07	-1.6674E-04	5.9876E-02	[260 K, Tc]
Thermal cond. liquid	2.7249E-15	-2.6039E-12	1.0791E-10	5.1634E-07	-4.5222E-04	2.2792E-01	[260 K, Tc]
Thermal cond. vapour	3.9207E-14	-6.3533E-11	4.0092E-08	-1.2122E-05	1.8122E-03	-1.0371E-01	[260 K, Tc]
Thermal cond. supercr.	-1.4297E-14	5.7388E-11	-9.1549E-08	7.2552E-05	-2.8464E-02	4.4578E+00	[Tc, 1000 K]
Density liquid	-3.2515E-10	5.1062E-07	-3.1726E-04	9.5229E-02	-1.4281E+01	1.6872E+03	[260 K, Tc]
Density vapour	1.8266E-10	-3.0025E-07	1.9986E-04	-6.6650E-02	1.1069E+01	-7.3000E+02	[260 K, Tc]
Density supecritical	-7.1955E-11	2.9348E-07	-4.7653E-04	3.8526E-01	-1.5529E+02	2.5073E+04	[Tc, 1000 K]
Saturation pressure	-9.4526E-07	2.9474E-03	-2.3799E+00	8.3051E+02	-1.3428E+05	8.2649E+06	[260 K, Tc]
Viscosity liquid	-3.2268E-08	7.1011E-05	-6.2517E-02	2.7558E+01	-6.1003E+03	5.4625E+05	[260 K, Tc]
Viscosity vapour	3.3759E-10	-5.7017E-07	3.8651E-04	-1.2978E-01	2.1473E+01	-1.3970E+03	[260 K, Tc]
Viscosity supercritical	-1.0535E-10	4.2221E-07	-6.7234E-04	5.3187E-01	-2.0917E+02	3.2912E+04	[Tc, 1000 K]

E25

Property	a_5	a_4	a_3	a_2	a_1	a_0	validity range
Enthalpy liquid	1.7311E-07	-2.7347E-04	1.7038E-01	-4.9868E+01	8.4763E+03	-9.9193E+05	[260 K, Tc]
Enthalpy vapour	-3.9949E-07	6.4719E-04	-4.1102E-01	1.2909E+02	-1.8830E+04	1.1473E+06	[260 K, Tc]

Enthalpy supercritical	1.3527E-07	-5.4138E-04	8.6039E-01	-6.7782E+02	2.6747E+05	-4.1848E+07	[Tc, 1000 K]
Latent heat vaporization	-5.7260E-07	9.2066E-04	-5.8141E-01	1.7895E+02	-2.7307E+04	2.1393E+06	[260 K, Tc]
Cp liquid	7.7856E-09	-1.2122E-05	7.3693E-03	-2.1755E+00	3.1494E+02	-1.6375E+04	[260 K, Tc]
Cp vapour	4.9033E-09	-7.6599E-06	4.6719E-03	-1.3863E+00	2.0391E+02	-1.0984E+04	[260 K, Tc]
Cp supercritical	-8.8126E-10	3.6250E-06	-5.9331E-03	4.8296E+00	-1.9537E+03	3.1688E+05	[Tc, 1000 K]
Cv liquid	1.7769E-09	-2.8187E-06	1.7310E-03	-5.1223E-01	7.5982E+01	-3.2165E+03	[260 K, Tc]
Cv vapour	1.5516E-09	-2.4335E-06	1.4896E-03	-4.4339E-01	6.8250E+01	-3.4121E+03	[260 K, Tc]
Cv supercritical	-2.0146E-10	8.3095E-07	-1.3615E-03	1.1068E+00	-4.4427E+02	7.2883E+04	[Tc, 1000 K]
Entropy liquid	3.4937E-10	-5.7955E-07	3.7980E-04	-1.1904E-01	2.3237E+01	-3.0447E+03	[260 K, Tc]
Entropy vapour	9.0677E-10	-1.8806E-06	1.4622E-03	-5.2111E-01	8.3026E+01	-3.4340E+03	[260 K, Tc]
Entropy supercritical	3.1154E-10	-1.2381E-06	1.9551E-03	-1.5346E+00	6.0479E+02	-9.4612E+04	[Tc, 1000 K]
Surface tension	5.1846E-16	-4.3609E-13	1.1956E-10	1.8710E-08	-1.2228E-04	5.6674E-02	[260 K, Tc]
Thermal cond. liquid	2.7147E-15	-2.5081E-12	-6.1016E-12	5.7638E-07	-4.7170E-04	2.3135E-01	[260 K, Tc]
Thermal cond. vapour	4.0936E-14	-6.5978E-11	4.1397E-08	-1.2443E-05	1.8481E-03	-1.0490E-01	[260 K, Tc]
Thermal cond. supercr.	-1.4987E-14	6.0076E-11	-9.5691E-08	7.5710E-05	-2.9652E-02	4.6350E+00	[Tc, 1000 K]
Density liquid	-3.4972E-10	5.4755E-07	-3.3883E-04	1.0128E-01	-1.5092E+01	1.7285E+03	[260 K, Tc]
Density vapour	1.8979E-10	-3.1062E-07	2.0576E-04	-6.8273E-02	1.1281E+01	-7.4018E+02	[260 K, Tc]
Density supecritical	-7.8044E-11	3.1751E-07	-5.1410E-04	4.1435E-01	-1.6644E+02	2.6764E+04	[Tc, 1000 K]
Saturation pressure	5.3900E-07	6.6689E-04	-9.9075E-01	4.1216E+02	-7.2137E+04	4.6287E+06	[260 K, Tc]
Viscosity liquid	2.4938E-10	-4.1289E-07	2.7689E-04	-9.2413E-02	1.5242E+01	-9.9055E+02	[260 K, Tc]
Viscosity vapour	5.7985E-10	-9.2893E-07	5.8430E-04	-1.7882E-01	2.6513E+01	-1.5206E+03	[260 K, Tc]
Viscosity supercritical	-1.0454E-10	4.1861E-07	-6.6598E-04	5.2632E-01	-2.0677E+02	3.2504E+04	[Tc, 1000 K]

E50

Property	a_5	a_4	a_3	a_2	a_1	a_0	validity range
Enthalpy liquid	1.6475E-07	-2.4871E-04	1.4937E-01	-4.2314E+01	7.4730E+03	-9.8771E+05	[260 K, Tc]
Enthalpy vapour	-6.6245E-07	1.0594E-03	-6.6273E-01	2.0348E+02	-2.9422E+04	1.8165E+06	[260 K, Tc]
Enthalpy supercritical	1.1926E-07	-4.7615E-04	7.5486E-01	-5.9320E+02	2.3384E+05	-3.6474E+07	[Tc, 1000 K]
Latent heat vaporization	-8.2721E-07	1.3081E-03	-8.1210E-01	2.4579E+02	-3.6895E+04	2.8042E+06	[260 K, Tc]
Cp liquid	1.0139E-08	-1.5457E-05	9.2050E-03	-2.6618E+00	3.7609E+02	-1.9024E+04	[260 K, Tc]
Cp vapour	6.2032E-09	-9.4952E-06	5.6777E-03	-1.6520E+00	2.3727E+02	-1.2529E+04	[260 K, Tc]
Cp supercritical	-9.7260E-10	3.9825E-06	-6.4868E-03	5.2539E+00	-2.1147E+03	3.4108E+05	[Tc, 1000 K]
Cv liquid	1.3053E-09	-1.9838E-06	1.1613E-03	-3.2394E-01	4.5185E+01	-1.0428E+03	[260 K, Tc]
Cv vapour	1.3469E-09	-2.0321E-06	1.1996E-03	-3.4435E-01	5.1845E+01	-2.3264E+03	[260 K, Tc]
Cv supercritical	-2.1245E-10	8.7318E-07	-1.4253E-03	1.1543E+00	-4.6182E+02	7.5461E+04	[Tc, 1000 K]
Entropy liquid	3.5568E-10	-5.8663E-07	3.9131E-04	-1.2932E-01	2.7511E+01	-3.6875E+03	[260 K, Tc]

Entropy vapour	1.0293E-09	-2.2547E-06	1.8273E-03	-6.7801E-01	1.1288E+02	-5.0944E+03	[260 K, Tc]
Entropy supercritical	-2.3013E-10	9.0341E-07	-1.4022E-03	1.0733E+00	-3.9872E+02	5.8550E+04	[Tc, 1000 K]
Surface tension	7.5725E-16	-1.1841E-12	7.4076E-10	-2.2047E-07	-6.7909E-05	5.0489E-02	[260 K, Tc]
Thermal cond. liquid	3.1801E-15	-2.9227E-12	3.4189E-11	6.7805E-07	-5.4298E-04	2.4849E-01	[260 K, Tc]
Thermal cond. vapour	5.5186E-14	-8.7710E-11	5.4263E-08	-1.6122E-05	2.3589E-03	-1.3152E-01	[260 K, Tc]
Thermal cond. supercr.	-1.2965E-14	5.1772E-11	-8.2138E-08	6.4726E-05	-2.5227E-02	3.9283E+00	[Tc, 1000 K]
Density liquid	-4.9554E-10	7.7054E-07	-4.7212E-04	1.3992E-01	-2.0503E+01	2.0215E+03	[260 K, Tc]
Density vapour	1.3866E-01	-2.0222E-07	1.1886E-04	-3.4829E-02	5.0520E+00	-2.8874E+02	[260 K, Tc]
Density supecritical	-6.0799E-11	2.4712E-07	-3.9981E-04	3.2208E-01	-1.2939E+02	2.0843E+04	[Tc, 1000 K]
Saturation pressure	2.8957E-06	-2.7703E-03	1.0062E+00	-1.6511E+02	1.0717E+04	-8.3030E+04	[260 K, Tc]
Viscosity liquid	-3.5727E-08	7.7079E-05	-6.6590E-02	2.8831E+01	-6.2751E+03	5.5324E+05	[260 K, Tc]
Viscosity vapour	5.4259E-10	-9.1774E-07	6.2265E-04	-2.0983E-01	3.4981E+01	- 2.3037e+03	[260 K, Tc]
Viscosity supercritical	-9.8962E-11	3.9451E-07	-6.2467E-04	4.9120E-01	-1.9197E+02	3.0030E+04	[Tc, 1000 K]

E85

Property	a_5	a_4	a_3	a_2	a_1	a_0	validity range
Enthalpy liquid	4.7358E-07	-7.3049E-04	4.4418E-01	-1.3067E+02	2.0942E+04	-1.9002E+06	[260 K, Tc]
Enthalpy vapour	-8.1068E-07	1.2617E-03	-7.6931E-01	2.3004E+02	-3.2454E+04	2.1621E+06	[260 K, Tc]
Enthalpy supercritical	1.6292E-07	-6.3091E-04	9.7087E-01	-7.4146E+02	2.8377E+05	-4.2856E+07	[Tc, 1000 K]
Latent heat vaporization	-1.2843E-06	1.9922E-03	-1.2135E+00	3.6071E+02	-5.3396E+04	4.0623E+06	[260 K, Tc]
Cp liquid	9.8215E-09	-1.4384E-05	8.2455E-03	-2.2931E+00	3.1030E+02	-1.3988E+04	[260 K, Tc]
Cp vapour	7.4905E-09	-1.1157E-05	6.4980E-03	-1.8421E+00	2.5678E+02	-1.3091E+04	[260 K, Tc]
Cp supercritical	-8.6984E-10	3.5549E-06	-5.7790E-03	4.6716E+00	-1.8771E+03	3.0267E+05	[Tc, 1000 K]
Cv liquid	1.4443E-09	-2.1424E-06	1.2160E-03	-3.2355E-01	4.0393E+01	1.2451E+02	[260 K, Tc]
Cv vapour	1.1517E-09	-1.6466E-06	9.2410E-04	-2.5122E-01	3.6129E+01	-1.2068E+03	[260 K, Tc]
Cv supercritical	-1.9674E-10	8.0806E-07	-1.3175E-03	1.0656E+00	-4.2589E+02	6.9730E+04	[Tc, 1000 K]
Entropy liquid	1.0457E-09	-1.7135E-06	1.1268E-03	-3.7256E-01	7.0476E+01	-7.1510E+03	[260 K, Tc]
Entropy vapour	1.4201E-09	-3.2285E-06	2.7039E-03	-1.0433E+00	1.8213E+02	-8.9583E+03	[260 K, Tc]
Entropy supercritical	-2.5933E-11	9.7572E-08	-1.4024E-04	9.3255E-02	-2.1477E+01	1.4440E+03	[Tc, 1000 K]
Surface tension	-5.5959E-15	8.6640E-12	-5.2722E-09	1.5472E-06	-3.0180E-04	5.9462E-02	[260 K, Tc]
Thermal cond. liquid	4.1467E-15	-3.8369E-12	1.9217E-10	8.4793E-07	-6.7871E-04	2.8178E-01	[260 K, Tc]
Thermal cond. vapour	5.5763E-14	-8.6451E-11	5.2189E-08	-1.5120E-05	2.1652E-03	-1.1705E-01	[260 K, Tc]
Thermal cond. supercr.	-1.1925E-14	4.7249E-11	-7.4337E-08	5.8062E-05	-2.2399E-02	3.4542E+00	[Tc, 1000 K]
Density liquid	-4.6292E-10	6.9879E-07	-4.1714E-04	1.2051E-01	-1.7262E+01	1.8175E+03	[260 K, Tc]
Density vapour	1.7493E-10	-2.5334E-07	1.4708E-04	-4.2466E-02	6.0643E+00	-3.4118E+02	[260 K, Tc]
Density supecritical	-9.8204E-11	3.8284E-07	-5.9365E-04	4.5792E-01	-1.7590E+02	2.7019E+04	[Tc, 1000 K]

Saturation pressure	3.6109E-06	-3.7570E-03	1.5233E+00	-2.9686E+02	2.7232E+04	-9.0367E+05	[260 K, Tc]
Viscosity liquid	-3.6368E-08	7.7061E-05	-6.5434E-02	2.7869E+01	-5.9723E+03	5.1920E+05	[260 K, Tc]
Viscosity vapour	4.7259E-10	-7.6140E-07	4.9400E-04	-1.5974E-01	2.5605E+01	-1.6227E+03	[260 K, Tc]
Viscosity supercritical	-8.6675E-11	3.4341E-07	-5.4019E-04	4.2181E-01	-1.6365E+02	2.5432E+04	[Tc, 1000 K]

Ethanol

Property	a_5	a_4	a_3	a_2	a_1	a_0	validity range
Enthalpy liquid	5.9190E-07	-9.0947E-04	5.5079E-01	-1.6199E+02	2.5876E+04	-2.2909E+06	[260 K, Tc]
Enthalpy vapour	-5.6598E-07	8.4974E-04	-5.0236E-01	1.4662E+02	-1.9857E+04	1.5986E+06	[260 K, Tc]
Enthalpy supercritical	2.1530E-07	-8.1308E-04	1.2211E+00	-9.1109E+02	3.4048E+05	- 5.0171e+07	[Tc, 1000 K]
Latent heat vaporization	-1.1579E-06	1.7592E-03	-1.0531E+00	3.0861E+02	-4.5733E+04	3.8895E+06	[260 K, Tc]
Cp liquid	5.8539E-08	-1.0183E-04	7.0351E-02	-2.4088E+01	4.0873E+03	-2.7211E+05	[260 K, Tc]
Cp vapour	4.9220E-08	-8.5802E-05	5.9336E-02	-2.0331E+01	3.4531E+03	-2.3141E+05	[260 K, Tc]
Cp supercritical	-1.6389E-09	6.3673E-06	-9.8577E-03	7.6037E+00	-2.9221E+03	4.5036E+05	[Tc, 925 K]
Cv liquid	1.8080E-09	-2.7060E-06	1.5453E-03	-4.1219E-01	4.9879E+01	2.7579E+02	[260 K, Tc]
Cv vapour	2.7591E-09	-4.5538E-06	3.0071E-03	-9.8790E-01	1.6417E+02	-9.9206E+03	[260 K, Tc]
Cv supercritical	-3.0848E-10	1.2103E-06	-1.8913E-03	1.4708E+00	-5.6774E+02	8.9434E+04	[Tc, 925 K]
Entropy liquid	1.3584E-09	-2.2288E-06	1.4711E-03	-4.9163e-01	9.3310e+01	-9.2149e+03	[260 K, Tc]
Entropy vapour	1.3256E-09	-3.1857E-06	2.7812E-03	-1.1126E+00	2.0028E+02	-9.7923E+03	[260 K, Tc]
Entropy supercritical	7.2876E-10	-2.7264E-06	4.0544E-03	-2.9976E+00	1.1080E+03	-1.6191E+05	[Tc, 1000 K]
Surface tension	-5.8423E-15	8.8246E-12	-5.2665E-09	1.5096E-06	-2.8376E-04	5.6515e-02	[260 K, Tc]
Thermal cond. liquid	4.7539E-15	-4.4032E-12	2.8050E-10	9.5804E-07	-7.6264E-04	3.0186E-01	[260 K, Tc]
Thermal cond. vapour	3.4768E-14	-5.2045E-11	3.0326E-08	-8.3993E-06	1.1704E-03	-5.9804E-02	[260 K, Tc]
Thermal cond. supercr.	-7.0440E-15	2.7995E-11	-4.4216E-08	3.4711E-05	-1.3427E-02	2.0883E+00	[Tc, 1000 K]
Density liquid	-5.5948E-10	8.4855E-07	-5.0730E-04	1.4673E-01	-2.0914E+01	2.0127E+03	[260 K, Tc]
Density vapour	2.1416E-10	-3.1909E-07	1.9041E-04	-5.6540E-02	8.3166E+00	-4.8302E+02	[260 K, Tc]
Density supecritical	-1.5690E-10	5.9206E-07	-8.8851E-04	6.6307E-01	-2.4626E+02	3.6509E+04	[Tc, 1000 K]
Saturation pressure	2.5162E-06	-2.5876E-03	1.0336E+00	-1.9872E+02	1.8161E+04	-6.1842E+05	[260 K, Tc]
Viscosity liquid	-2.7251E-08	5.8433E-05	-5.0275E-02	2.1722E+01	-4.7285E+03	4.1848E+05	[260 K, Tc]
Viscosity vapour	5.0521E-10	-8.1921E-07	5.3490E-04	-1.7427E-01	2.8189E+01	- 1.8058e+03	[260 K, Tc]
Viscosity supercritical	1.1667E-10	-4.2729E-07	6.1940E-04	-4.4365E-01	1.5668E+02	-2.1598E+04	[Tc, 1000 K]

List of figures and Captions

engines: cold-start, idle, part-load, and wide-open-throttle (WOT) operations.

Figure 22: Calculated variation in vapour pressure due to temperature and non-ideal blending, with respect of the loci of typical chamber pressures for a GDI engine, which is represented by a shaded area.

List of tables and captions

Table 1: composition used by Ref. [22] for the RVP and for calculation reported in figure 3, and critical parameters of single component.

Table 2: compositions used by Ref.[30] to simulate the distillation characteristics of real-like fuels

Table 3: main characteristics of the surrogate components used in modelling

Table 4: compositions of the fuel surrogates used in modelling in mole fractions.

Table 5: Calculated critical parameters, temperatures and Reid vapour pressure of the fuel surrogates used in modelling.

Table 6: Comparison of calculations of saturation properties for ethanol and indolene with selected data from literature.

Table of coefficients: see the attached table containing the 1296 coefficients in Appendix A.